JOURNAL OF GEOPHYSICAL RESEARCH, VOL. 114, D18205, doi:10.1029/2008JD011188, 2009

An approach to estimate global biomass burning emissions of organic and black carbon from MODIS fire radiative power

Eric Vermote,[1] Evan Ellicott,[1] Oleg Dubovik,[2] Tatyana Lapyonok,[3,4] Mian Chin,[5] Louis Giglio,[4] and Gareth J. Roberts[6]

Received 23 September 2008; revised 29 May 2009; accepted 17 June 2009; published 23 September 2009.

[1] Biomass burning is the main global source of fine primary carbonaceous aerosols in the form of organic carbon (OC) and black carbon (BC). We present an approach to estimate biomass burning aerosol emissions based on the measurement of radiative energy released during combustion. We make use of both Aqua and Terra MODIS observations to estimate the fire radiative energy using a simple model to parameterize the fire diurnal cycle based on the long-term ratio between Terra and Aqua MODIS FRP. The parameterization is developed using cases of frequent (up to 12 times daily) MODIS observations, geostationary data from SEVIRI, and precessing observations from TRMM VIRS. FRE-based emission coefficients for the organic and black carbon (OCBC) component of fine mode aerosols are computed from multiple regions encompassing grassland/savanna, tropical forest, and extratropical forest biomes using OCBC emission estimates derived from the MODIS fine mode aerosol product and an inverse aerosol transport model. The values of emission coefficients for OCBC retrieved were 2.7 ± 0.3 g/MJ for grassland/savanna, 8.6 ± 0.8 g/MJ for tropical forest, and 14.4 ± 0.8 g/MJ for extratropical forest. The FRE monthly data are then used to estimate OCBC emissions from biomass burning on a global basis. For 2001 to 2007, our annual estimates are comparable to previously published values. According to our estimate, the OCBC emissions are the largest for 2003 (18.8 Tg), roughly 20% above average and primarily driven by wildland fires in the Lake Baikal region (Russia).

Citation: Vermote, E., E. Ellicott, O. Dubovik, T. Lapyonok, M. Chin, L. Giglio, and G. J. Roberts (2009), An approach to estimate global biomass burning emissions of organic and black carbon from MODIS fire radiative power, *J. Geophys. Res.*, *114*, D18205, doi:10.1029/2008JD011188.

1. Introduction

[2] Biomass burning is recognized as a significant source of atmospheric trace gas and particulate matter emissions [*Crutzen and Andreae*, 1990] and has received attention from the scientific community over the past several decades as an important contributor to total climatic radiative forcing [*Innes*, 2000; *Kaufman et al.*, 1990].

[3] Aerosols influence Earth's radiative balance through scattering and absorbing the shortwave radiation. The *IPCC* [2007] reports the direct radiative forcing impact of biomass burning aerosols as 0.03 Wm^{-2}, with approximately a factor of 4 uncertainty (±0.12) In addition, aerosols can influence Earth's climate in more complex and indirect pathways such as changing cloud albedo and lifetime. However, there is good deal of uncertainty in estimating the forcing effects of biomass burning aerosols, in part because of an incomplete understanding of the optical properties of smoke and aerosol-atmosphere interactions. A prerequisite to understanding these interactions at regional and global scales is reliable estimates of aerosol emissions from wildland fires, both spatially and temporally. Although efforts to quantify biomass burning emissions have improved over the past several decades the inaccuracies of input data and variations in the methodologies employed may lead to an uncertainty in emission estimates of at least 50% [*French et al.*, 2004; *Kasischke and Penner*, 2004; *Robinson*, 1989; *Schultz et al.*, 2008].

[4] *Soja et al.* [2004] and *French et al.* [2004] suggested that limited information about soil organic layer burning is potentially a significant source of error in biomass burning emission estimates. *Ito and Penner* [2005], using the Global Burned Area (GBA) product from the SPOT satellite, estimated 1428 Tg carbon (C) emitted from fires in 2000. For comparison, *Hoelzemann et al.* [2004], using the Global Burnt Scar (GLOBSCAR) burned area product generated from the ASTR satellite, estimated 1741 Tg C for the same

[1]Department of Geography, University of Maryland, College Park, Maryland, USA.
[2]Laboratory of Atmospheric Optics, University of Sciences and Technologies of Lille 1, Lille, France.
[3]Laboratory for Terrestrial Physics, NASA Goddard Space Flight Center, Greenbelt, Maryland, USA.
[4]Science Systems and Applications, Inc., Lanham, Maryland, USA.
[5]Laboratory for Atmospheres, NASA Goddard Space Flight Center, Greenbelt, Maryland, USA.
[6]Department of Geography, Kings College of London, London, UK.

0148-0227/09/2008JD011188$09.00

year. This is surprising given that the GBA burned area estimate by *Ito and Penner* [2005] was nearly twice as large as GLOBSCAR used by *Hoelzemann et al.* [2004] (314×10^6 ha and 172×10^6, respectively). *Kasischke and Penner* [2004] suggested that differences in fuel load estimates and combustion factors, in addition to burned area, were responsible for the disagreement in emission estimates. A comparison of carbon emission estimates from biomass burning for 2000 made by *van der Werf et al.* [2006] (2038 Tg C) and *Schultz et al.* [2008] (2254 Tg C) highlights additional variability in recent estimates.

[5] Organic and black carbon (OC and BC, respectively) are predominately generated from biomass burning [*Bond et al.*, 2004] and are associated with light scattering and absorbing properties, respectively. Relatively greater emissions of OC and BC come from forest fires than savanna fires owing to the larger proportions of smoldering combustion. (Note that we refer to OC + BC aerosol emissions as OCBC for the remainder of the paper). Global estimates of these fine mode aerosols emitted from biomass burning have greater uncertainties than trace gas emissions [*Andreae and Merlet*, 2001]. As an example, *van der Werf et al.* [2006] reported 22 Tg of OCBC in 2001, while *Chin et al.* [2007] reported 56.3 Tg for the same year. In their earlier work, *Chin et al.* [2002] estimated an annual average of 88 Tg OCBC for the 1990s. This higher estimate is in part due to the use of a larger emission factor (14 g/kg [2002] versus 8 g/kg [2007]) and larger estimate of biomass combusted (5510 Tg dry matter [2002] versus 4942 Tg dry matter [2007]). Other estimates of OCBC are reasonably consistent. *Hoelzemann et al.* [2004] reported 17.6 Tg of OCBC for 2000 with a range of 13.6–20.2 Tg. *Schultz et al.* [2008] developed a 40 year inventory of vegetation fire emissions using a combination of burned area estimates from satellite products, data reported in the literature, and modeling which yielded an OCBC annual mean for the 1990s of 25 Tg. *Andreae and Merlet* [2001] reported 26.1 Tg of OCBC emitted from fires for the late 1990s while *Bond et al.* [2004] had 26.3 Tg OC for a "typical" year in the 1990s. However, it should be noted that most of these estimates relied in some part, if not directly, on emission factors reported by *Andreae and Merlet* [2001], suggesting that agreement between estimates is often a result of use of common data, and thus similar in biases [*Robinson*, 1989]. Differences may therefore be attributed to variations in other modeling components such as fuel loads or burned area. The uncertainty in each of these estimates is at least 50%, and possibly much greater [*Kasischke and Penner*, 2004; *Schultz et al.*, 2008].

[6] It is not surprising then that current uncertainty surrounding the impact of aerosol forcing is, according to the International Global Observation Strategy (IGOS), "one of the largest unknown factors in climate research" and is in large part due to poor estimates of the contribution from biomass burning [*Barrie et al.*, 2004].

[7] In part, the variation in emission estimates can be attributed to the methodologies employed. A common approach, referred to in this paper as "bottom up", is based on estimates of surface variables (total fuel consumption per unit area, the area burned, and the type of fuel affected) that are used to compute emissions to the atmosphere. On the other hand, "top down" (inversion) approaches seek to measure atmospheric constituent concentration associated with fire (e.g., CO, aerosols) to estimate emission sources at the surface.

[8] Earth observing satellites have made a significant contribution to wildfire detection, monitoring, and characterization for nearly two decades [*Dozier*, 1981; *García et al.*, 1991; *Kasischke et al.*, 1995a, 1995b; *Kaufman et al.*, 1990; *Korontzi et al.*, 2004; *Robinson*, 1991; *van der Werf et al.*, 2003, 2006; *Wooster et al.*, 2003, 2005]. Current satellite based, bottom-up approaches to estimate emissions involve multiplying the fuel consumed by an a priori emission factor for the atmospheric species (gas or aerosol) of interest (equation (1)):

$$E_x = EF_x \times M \tag{1}$$

Where E_x is the emission load of species x (g); EF_x is the emission factor for species x for the specific vegetation type or biome (g kg^{-1}); and M is the biomass burned (kg). The biomass burned is calculated using equation (2).

$$M = A \times B \times \beta \tag{2}$$

Where A is the burned area (km^2); B is the biomass or fuel load (kg km^{-2}); and β is combustion factor (fraction of available fuel burned).

[9] The combustion factor cannot be measured from space and the uncertainty in space-based measurements of burned area and fuel loads is high [*van der Werf et al.*, 2006]. *Boschetti et al.* [2004] showed that differences in spatial and temporal estimates of burned area were apparent between the GLOBSCAR and GBA2000 products with the latter producing a global burned area nearly twice as large as GLOBSCAR. They concluded that such discrepancies have serious implications for accurately quantifying emissions from fires [*Boschetti et al.*, 2004]. *Korontzi et al.* [2004] showed that estimates of burned area for southern Africa can vary significantly between burned area algorithms, which when coupled with the landcover types that are burning, can result in differences in the amount of biomass consumed exceeding a factor of two. The difficulty in accurately measuring these variables leads to an uncertainty in emission estimates of at least 50% [*French et al.*, 2004; *Andreae and Merlet*, 2001; *Korontzi et al.*, 2004; *Robinson*, 1989; *van der Werf et al.*, 2003]. Although data sets used for this application are continuously improved [*Roy et al.*, 2005; *van der Werf et al.*, 2006], because of the uncertainty in current estimates it is worthwhile to explore other approaches.

[10] In this work we investigate the relationship between detected fire radiative energy (FRE) and emissions. We demonstrate an approach to estimate instantaneous FRE (MJ s^{-1}), or "fire radiative power" (FRP), from MODIS observations for multiple years. We employ high temporal frequency observations from SEVIRI and VIRS, as well as high-latitude retrievals made by MODIS, to aid in characterizing the diurnal cycle of FRP. The relationship between the diurnal cycle and the ratio of Terra-MODIS and Aqua-MODIS FRP measurements is explored as a method to parameterize the fire energy temporal trajectory. We then calculate FRE, using only MODIS data, as the integral of discrete FRP estimates. Next we explore the relationship

between the estimated FRE and a new MODIS-derived inversion product of daily integrated, biomass burning aerosol emissions. The inversion product is generated from the MODIS fine mode aerosol optical thickness and inverse modeling transport processes adopted from the Goddard Chemistry Aerosol Radiation and Transport (GOCART) model. Fine mode aerosols are defined as particles with an aerodynamic diameter less than 2.5 μm (PM2.5). The inversion yields the sources (locations and intensities) of fine mode aerosols [*Dubovik et al.*, 2008] attributed to biomass burning. The fine mode aerosol optical thickness is converted to mass using a 7.6 ± 1.9 m^2/g (see section 5) conversion factor and then OCBC mass is estimated on the basis of the proportion of PM2.5 mass which is composed of OCBC (average of 0.68 ± 0.15) which was reported by *Andreae and Merlet* [2001] for the three biomes considered in this study. Although it would appear that emission estimates could just be made utilizing the inversion product, the process is still rather time-consuming and not intended for an operational approach.

[11] In our global analysis we chose to follow a similar approach by *van der Werf et al.* [2006] to determine emission coefficients. The relationship between estimated FRE and the inversion-based OCBC product is investigated within 3 globally dispersed vegetation zones (biomes). The slope of the relationship within each biome is used as the representative emission coefficient to estimate OCBC from FRE. As previously stated, this type of generalization will incur a degree of uncertainty. In addition, as we mentioned earlier, there is incomplete understanding of aerosol optical properties which implies a level of uncertainty in any emission estimate. These issues are addressed in our error budget.

[12] An overview of the data and products used in this research is provided in section 2. The methodology used to calculate FRE and subsequent results are described in section 3. We then discuss our approach to generate FRE-based emission coefficients in section 4. Section 5 offers a review of the potential sources and magnitude of error in our data and estimates. Results are provided and discussed in section 6 with concluding remarks in section 7.

2. Data

2.1. MODIS FRP

[13] The MODIS sensors, onboard the sun-synchronous polar-orbiting satellites Terra and Aqua, acquire four observations of nearly the entire Earth daily at 1030 and 2230 (Terra) and 0130 and 1330 (Aqua), equatorial local time. The first MODIS sensor was launched aboard the Terra satellite in 1999; the second was launched in 2002 aboard Aqua.

[14] We used one year (2003) of data from the MODIS Aqua Climate Modeling Grid (CMG) Collection 5. The CMG product provides monthly mean fire radiative power, as well as products describing cloud fraction and corrected pixel counts, at 0.5° spatial resolution [*Giglio*, 2005; *Giglio et al.*, 2006]. Monthly mean FRP was multiplied by the cloud-and-overpass–corrected fire pixel count, producing the total FRP released within a given grid cell for each time period. The CMG monthly product was used to estimate FRE, compare with a biomass burning emissions product (described below in section 2.4), derive emission coefficients, and ultimately predict OCBC emissions from fire. We also used 5 years of monthly CMG data (2003 to 2007) from both Terra and Aqua to offer a long-term (rather than a single year) characterization of the temporal variability between the two satellite observations. This variability is used later to parameterize the fire radiative energy diurnal cycle.

[15] In addition, we used the MODIS Level 2 fire product (MOD14) for Terra and Aqua. This fire product is collected daily at 1 km resolution and includes, among other information, the latitude, longitude, FRP, and confidence of the fire detection. Since neither SEVIRI nor VIRS provide high-latitude fire observations (i.e., boreal fires) the fire radiative energy diurnal cycle characterization for this case was supplemented by MODIS observations and is described later in section 3.1.

2.2. SEVIRI FRP

[16] SEVIRI was launched aboard the European Organization for the Exploitation of Meteorological Satellites (EUMETSAT) Meteosat-8 satellite on 28 August 2002. SEVIRI's nominal position at 0° longitude centers it on Europe and Africa while providing a geographic viewing range between approximately 75°E–75°W and 75°N–75°S in the longitudinal and latitudinal directions, respectively. The SEVIRI sensor provides 15-minute temporal resolution across 11 spectral channels (0.6 μm–14 μm) with a horizontal spatial resolution of 3 km at the sub-satellite point and an instantaneous field of view (IFOV) of 4.8 km. Of particular interest is the 3.9 μm "fire" channel, which has a low noise-equivalent temperature difference (NEdT) of less than 0.35 k at 300 k [*Roberts et al.*, 2005]. We used SEVIRI FRP observations from February and July 2004. These two months capture the distinct period of fire activity in Africa which follows a latitudinal gradient, starting in the North and progressing South through the year, eventually shifting North again by December. A large number of observations were available for February and July ($\sim 1.3 \times 10^6$ and 2.1×10^6 fire pixels, respectively) providing an adequate sample to characterize the fire radiative energy diurnal cycle (see Figure 3a).

2.3. TRMM VIRS

[17] The Visible and Infrared Scanner (VIRS) aboard the Tropical Rainfall Measuring Mission (TRMM) was launched in 1997 and though intended to monitor rainfall variability it has proven successful at fire detection and monitoring, owing to channel placements at 3.75 μm and 10.8 μm [*Giglio*, 2007; *Ji and Stocker*, 2002]. TRMM has an inclined (35°), precessing orbit so that VIRS observes the Earth between 38°N and 38°S. The precessing orbit also means that local overpass time changes to cover each hour of a day once per month. This drift in overpass time allowed *Giglio* [2007] to characterize the diurnal cycle of fire observations for a "typical" 24 hour period after corrections for overpass and cloud obscuration biases. We used the probability density functions (PDF) for 7 of the 15 diurnal cycles reported by *Giglio* [2007]. Although this data does not directly provide a quantity of FRP, the probability of fire detection for a given hour corresponds well with FRP as demonstrated by *Giglio* [2007]. Therefore it can be assumed

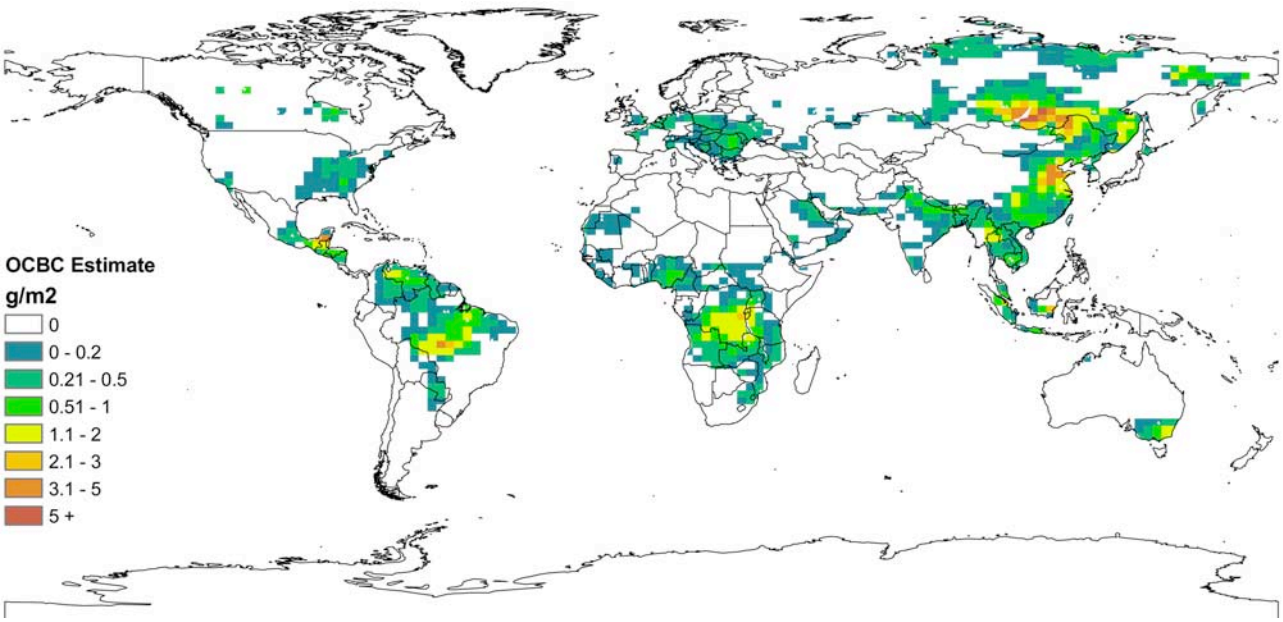

Figure 1. Organic and black carbon particulate matter emissions mass (g/m^2) for 2003 (30.5 Tg) estimated through observations from MODIS and inverse transport modeling with GOCART.

that the shape of the TRMM PDF curves corresponds with the shape of the FRP diurnal curve.

2.4. OCBC Emissions From Inverse Modeling

[18] Contrary to conventional approaches which rely on the emission inventories, this study incorporates OC and BC emission fields using global observations of aerosol from satellites. The distribution of fine mode aerosol optical thickness (AOT) derived from MODIS measurements allows global monitoring of the daily dynamics of biomass burning events. However, these AOT distributions do not provide the details regarding the exact locations and strength of the aerosol emission sources since the aerosol fields observed from satellites include both freshly emitted aerosol and aerosol emitted prior to the actual satellite overpass; the latter being redistributed and transformed by atmospheric processes (advections by winds, rain washout, deposition, etc.). Therefore this study relies on the information provided by inverse modeling that accounts for atmospheric processes and derives the aerosol emissions from satellite observations. Specifically, we used the aerosol source information retrieved through the algorithm by *Dubovik et al.* [2008] from MODIS fine mode aerosol AOT measurements.

[19] *Dubovik et al.* [2008] used the Goddard Chemistry Aerosol Radiation and Transport (GOCART) aerosol transport model to invert MODIS optical depth measurements to derive a spatially and temporally resolved description of surface fine mode aerosol sources. These aerosol sources include other species besides those produced from biomass burning, such as anthropogenic combustion (e.g., from coal burning), which represent a very small fraction in the regions of significant fire activity and can be neglected in our analysis. The fine mode aerosol is converted to PM2.5 mass by using the average value of 7.6 ± 1.9 m^2/g mass extinction coefficient (β_e) which relates the dry mass of particulate matter to the fine mode optical depth [*Chin et al.*, 2002]. Organic and black carbon mass was then estimated from the PM2.5 mass using an average fraction of 0.68 [*Andreae and Merlet*, 2001]. Organic carbon, associated with smoldering combustion, is characterized by light scattering properties and thus has implications for negative climate forcing. Black carbon, on the other hand, is generally a product of flaming combustion and dominates light absorption by aerosols, resulting in a positive climate forcing. The typical ratio of OC to BC adopted in this research is 7:1 [*Chin et al.*, 2002].

[20] Total OCBC emissions for 2003 (30.5 Tg) are shown in Figure 1. Regions of fire activity are clearly visible, including the Arc of Deforestation in Brazil, Central America (e.g., Yucatan Peninsula), Southeast Australia, Southern Africa, and Southeast Russia. There are regions where the OCBC product is not fully corrected for anthropogenic and biogenic sources which can be seen in Eastern China, Europe, and portions of the United States south of the Great Lakes.

[21] *Dubovik et al.* [2008] optimized the inversion process by employing adjoint modeling to reduce computational the burden of modeling back trajectories. Despite this, the inversion process is still time-consuming and not realistic as a near-real-time operational product. Therefore our approach to estimate emissions using FRE and FRE-based emission coefficients provides a simple and efficient method by combining the robustness of the inverse method with the temporal variability obtained from near real-time observations of FRE.

3. Fire Radiative Energy

3.1. Background

[22] The rate at which energy is emitted by a fire, or the fire radiative power (FRP) during combustion can serve as a proxy for the rate of gas and aerosol emissions released [*Kaufman et al.*, 1996, 1998]. Integrating the FRP over the lifespan of a fire event and multiplying this value by an emission coefficient (EC_x), which describes the quantity of gas or particulate matter emitted per MJ of energy released

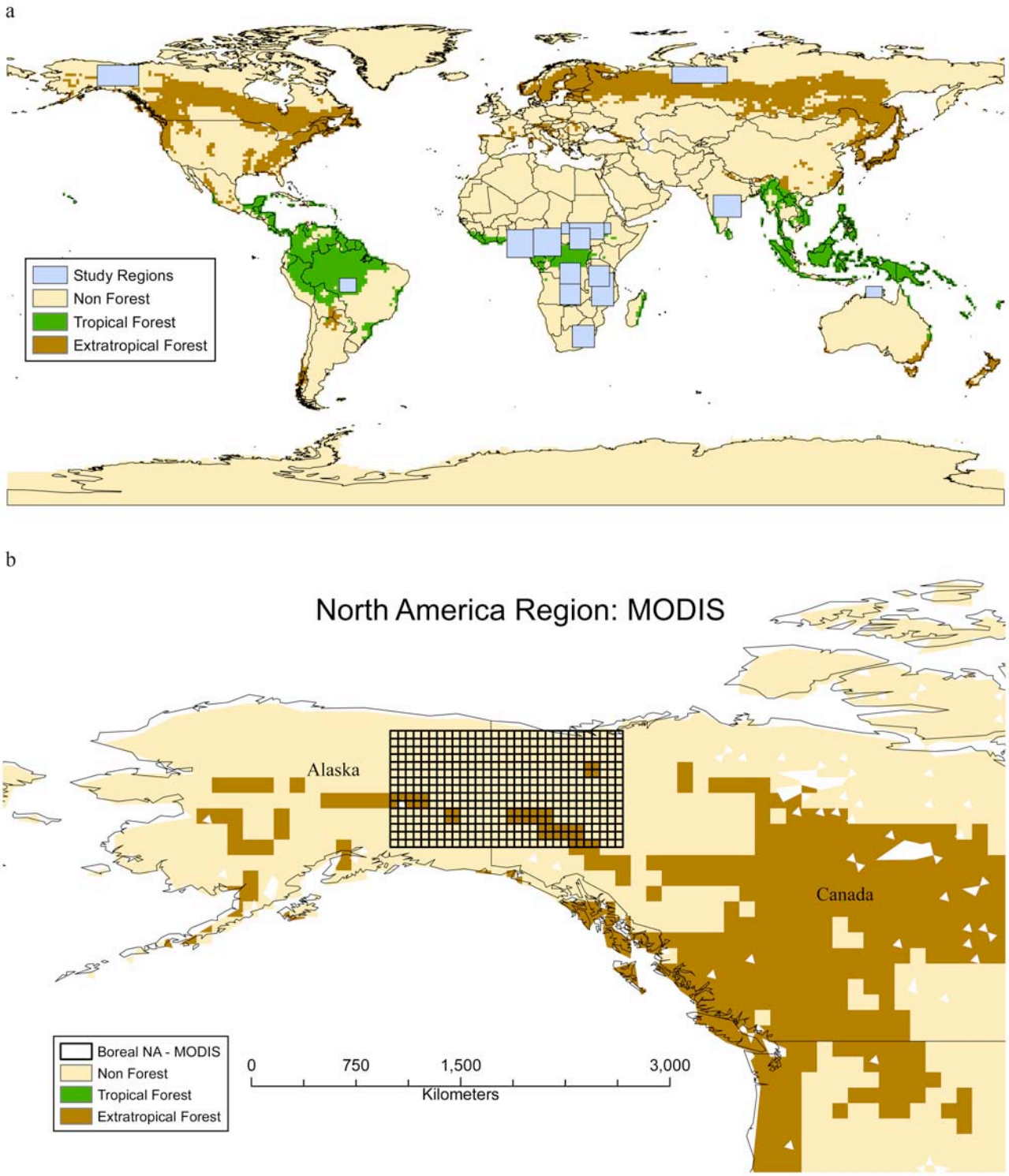

Figure 2. (a) Global extent of regions used to analyze the diurnal cycle from SEVIRI, TRMM, and MODIS observations. Sites are overlaid on the GFEDv2.1 vegetation map. (b–h) Zoomed look at the regions and corresponding vegetation categories. Figures 2b and 2c are for MODIS-based data; Figure 2d is the SEVIRI-based regions (note: red circle is shown to indicate the region used in Figure 3a); and Figures 2e through 2h are the TRMM VIRS regions.

(g/MJ), yields the total emissions from a fire (equation (3)):

$$Emission_x = EC_x \int FRP\, dt \tag{3}$$

(Note: We use the term *Emission Coefficient* rather than *Emission Factor* to avoid confusion between the former, which is in units of grams per energy released, and the latter which is in grams per mass of fuel consumed (g/kg)).

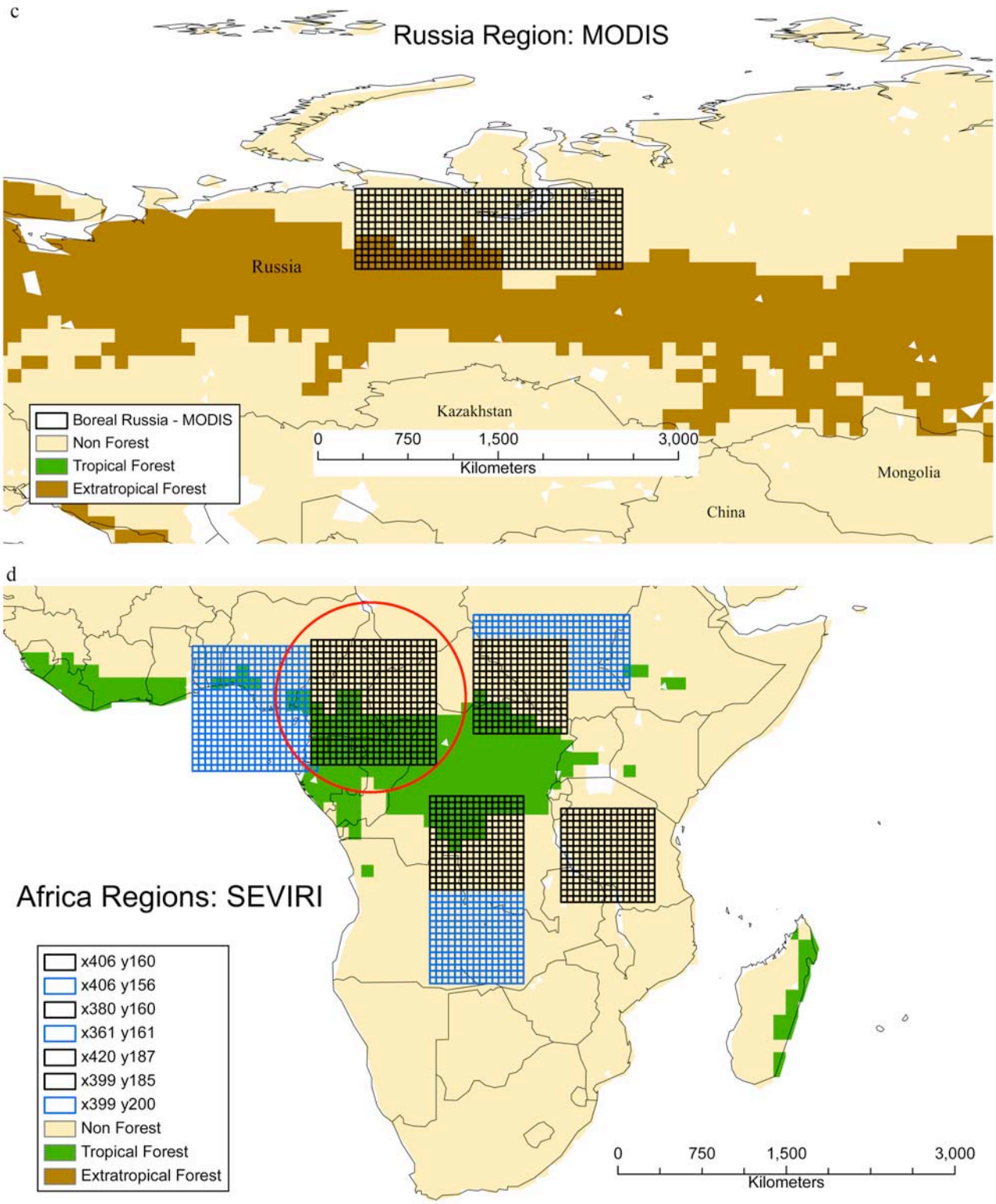

Figure 2. (continued)

[23] Using simulated cases of fire radiative energy, *Kaufman et al.* [1996, 1998] developed an empirical relationship between the fire energy and temperature measured by the middle infrared channel (3.9 μm) which forms the basis for the current FRP algorithm (equation (4)) used aboard the Moderate Resolution Imaging Spectroradiometer (MODIS):

$$\mathrm{FRP}\left[\mathrm{MW\,km^{-2}}\right] = 4.34 \times 10^{-19}\left(T^{8}_{\mathrm{MIR}} - T^{8}_{\mathrm{bg,MIR}}\right) \qquad (4)$$

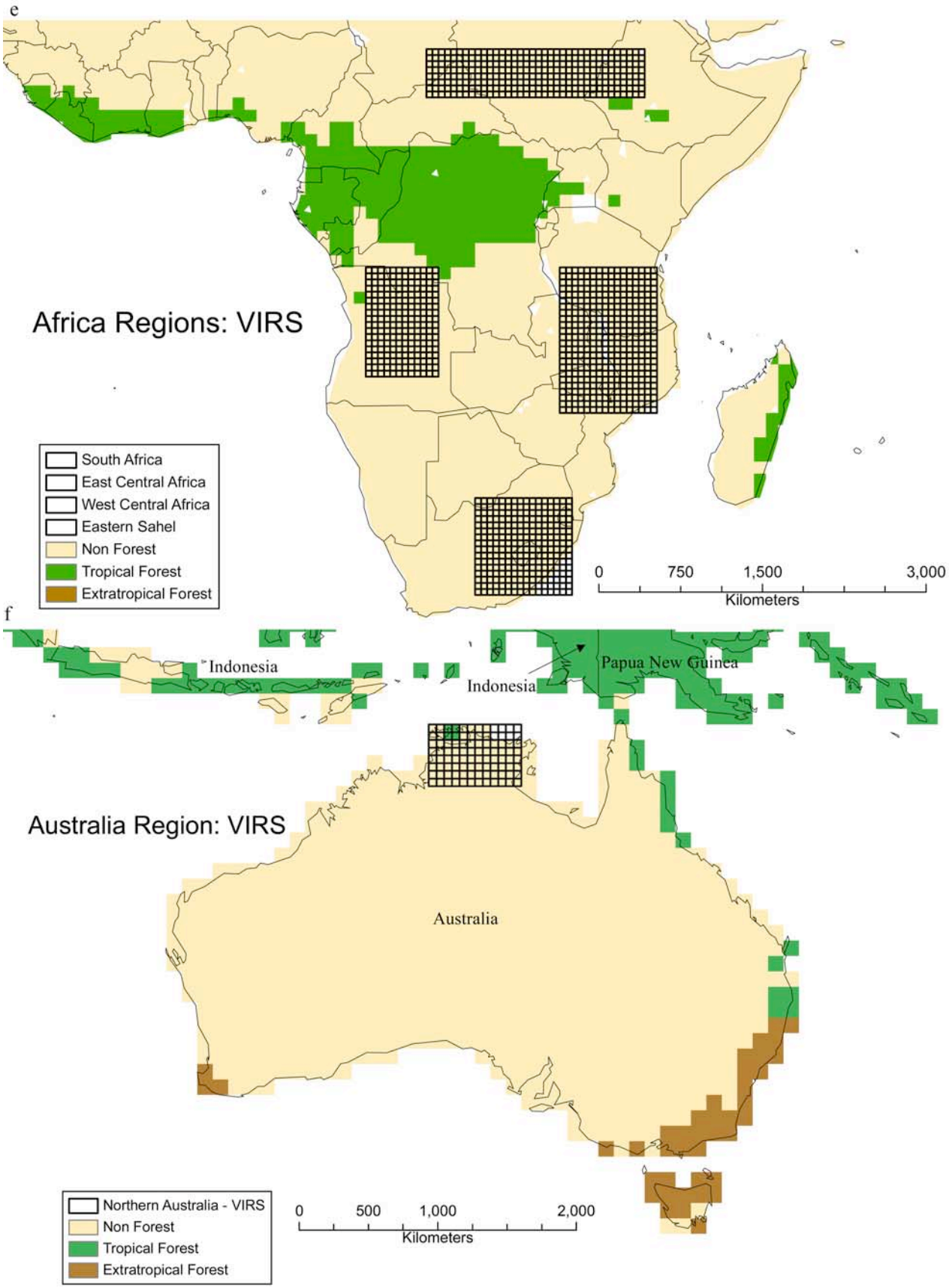

Figure 2. (continued)

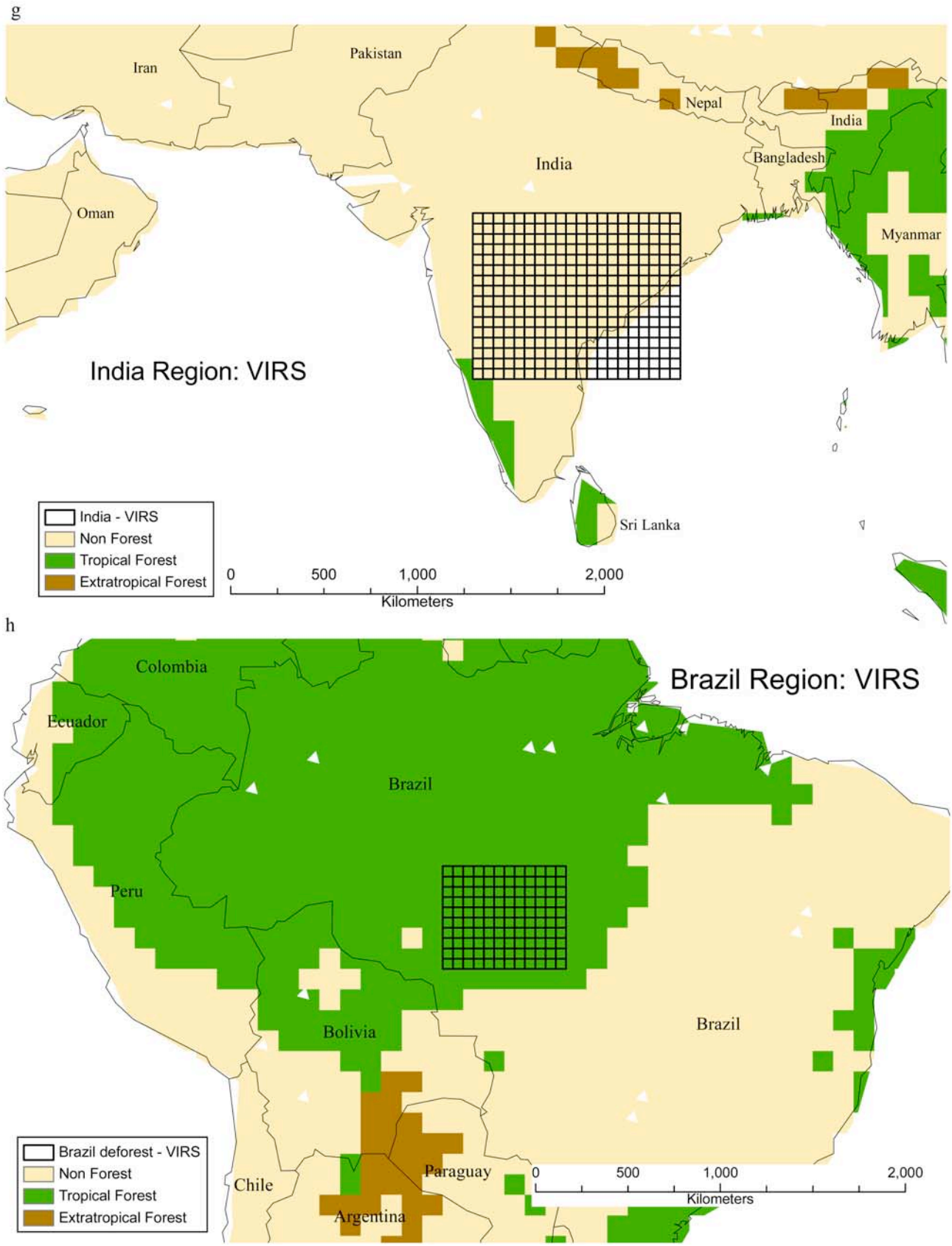

Figure 2. (continued)

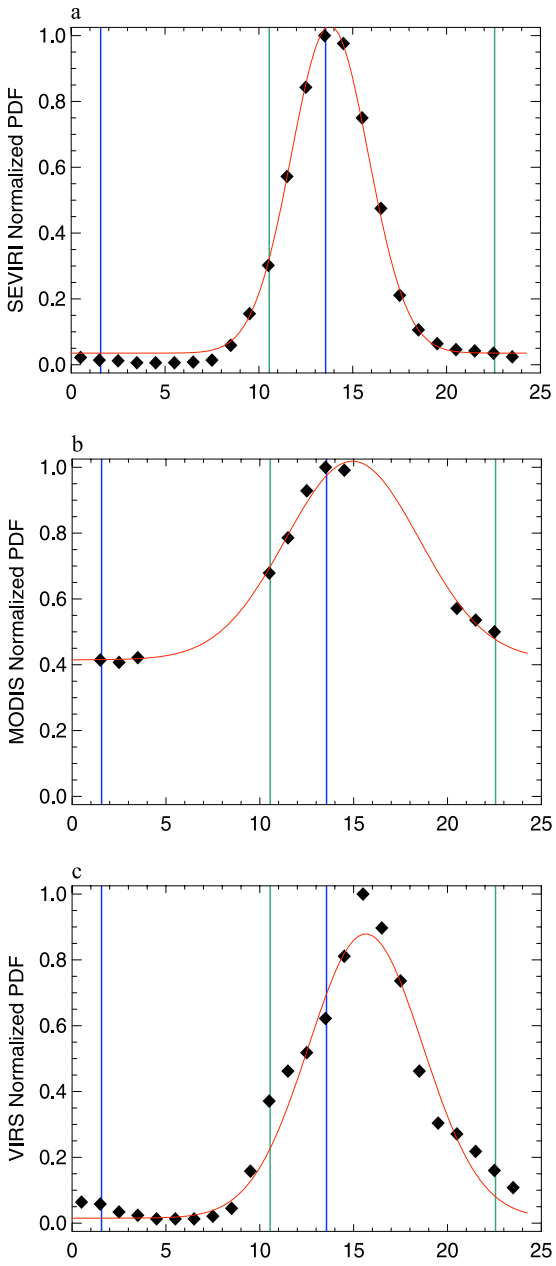

Figure 3. (a) SEVIRI, (b) MODIS, and (c) TRMM fire radiative energy diurnal cycles. The red curve (solid line) shows the fit of the diurnal cycle using a modified Gaussian function (equation (5)): Figure 5a is from a northern Africa study site (x380 y160, Figure 2d); Figure 5b is from boreal Russia (x480 y43, Figure 2c); and Figure 5c is the TRMM VIRS "Brazil deforestation" area (x240 y196, Figure 2h). Shown for reference are MODIS overpass times: green vertical lines for MODIS-Terra and blue vertical lines for MODIS-Aqua.

where FRP is the rate of radiative energy emitted per pixel (the MODIS 4 μm channel has IFOV of 1 km), 4.34 $\times$ 10^{-19} [MW km^{-2} Kelvin^{-8}] is the constant derived from the simulations, T_{MIR} [Kelvin] is the radiative brightness temperature of the fire component, $T_{\mathrm{bg,MIR}}$ [Kelvin] is the neighboring nonfire background component, and MIR refers to middle infrared wavelength, typically 4 μm. Simulations of the radiation emitted by pixels with different combinations of flaming and smoldering phases demonstrated that the retrieved fire energy using the empirical fit had a standard deviation of 16%. This value is later used in our error budget (section 5).

[24] *Wooster* [2002] investigated the relationship between FRP and fuel consumption using field measurements which provided supporting evidence for the effectiveness of using time integrated FRP, FRE, to estimate biomass burned. *Ichoku and Kaufman* [2005] used MODIS FRP and aerosol products to estimate near real time rates of aerosol emissions and FRP-based emission coefficients at regional scales. Recently, *Roberts and Wooster* [2008] employed FRP retrievals from African fires using SEVIRI to calculate the total fire energy and estimate total biomass consumed.

[25] The application of instantaneous and total FRE has potential in estimating combustion rates, total fuel consumed, and emissions released. However, to date, no study has employed this approach at a global scale.

3.2. Fire Energy Diurnal Cycle

[26] An important characteristic of the radiative energy emitted from fires is the diurnal cycle. *Giglio* [2007] characterized the hourly cycle of fire activity in the tropics and subtropics using the Visible and Infrared Scanner (VIRS) aboard the Tropical Rainfall Measuring Mission (TRMM) satellite. For most tropical and subtropical fires the temporal trajectory (or curve) follows a rather distinct pattern of increasing hourly fire activity into the early afternoon, followed by a rapid drop in activity (and associated fire radiative energy) through the evening. Describing the discrete observations as a continuous function simplifies quantifying the integral of the area beneath the curve which represents the total fire energy (FRE) detected. The application of geostationary observations from SEVIRI by *Roberts and Wooster* [2008] showcased the capability of high temporal FRP measurements for the calculation of time integrated fire energy. Here we offer an approach to estimate FRE from MODIS observations of FRP.

[27] Employing SEVIRI, TRMM, and MODIS data, the diurnal fire cycle was examined at sites that were large

Table 1. Climate Modeling Grid (CMG) Sites Used for Extracting the Terra/Aqua Ratio Over 5 Years of Observations (2003–2007)[a]

x (CMG)	y (CMG)	Size (degree)	Region Description
406	160	7.5° × 7.5°	SEVIRI: eastern sahel
406	156	12.5° × 6°	SEVIRI: eastern sahel
380	160	10° × 10°	SEVIRI: central
361	161	10° × 10°	SEVIRI: central coast
399	200	7.5° × 7.5°	SEVIRI: south central
420	187	7.5° × 7.5°	SEVIRI: south east
399	185	7.5° × 7.5°	SEVIRI: central
400	156	18° × 8°	VIRS: eastern sahel
390	192	6° × 9°	VIRS: west central Africa
240	196	6° × 5°	VIRS: Brazil deforest
422	192	8° × 12°	VIRS: east central Africa
620	202	6° × 4°	VIRS: northern Australia
408	230	8° × 8°	VIRS: South Africa
510	136	10° × 8°	VIRS: India
480	43	20° × 6°	MODIS: north central Russia
65	42	15° × 7.5°	MODIS: Alaska-Canada border

[a]The first and second columns are the upper left coordinate for each region; coordinates are in CMG 0.5° cell designation. The range for the CMG grid is 720 × 360. The size column gives the longitude × latitude size. The last column is the name give to the region.

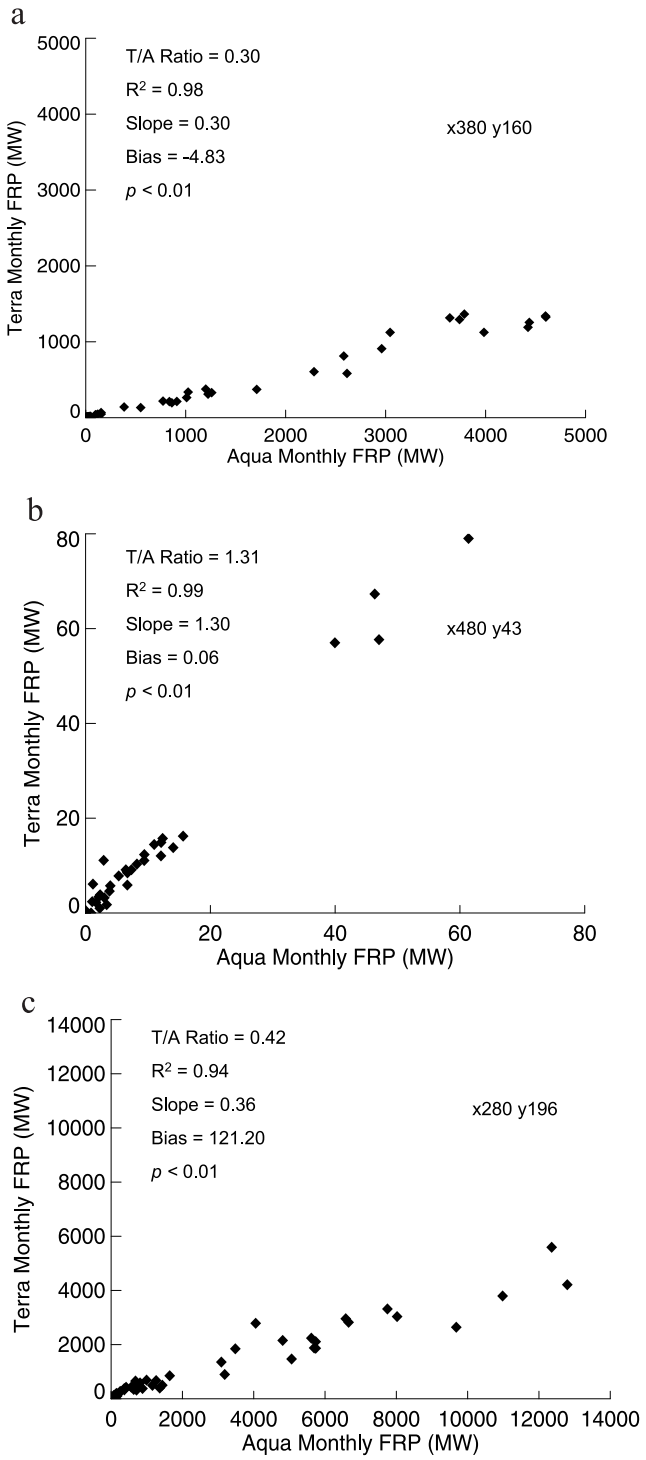

Figure 4. (a–c) Ratio between monthly Terra and Aqua (*T*/*A*) CMG FRP from 2003 to 2007 ($n = 60$) for study sites (see Figure 2a) used to develop relationship between *T*/*A* ratio and diurnal curve from higher temporal resolution observations. *XY* coordinates represent the upper left cell of the site based on the CMG (720 × 360). Figure 4a is in central Africa, corresponding with SEVIRI observations (corresponding with Figures 2d and 3a), Figure 4b corresponds with MODIS boreal diurnal curve site (corresponding with Figures 2c and 3b), and Figure 4c is the *T*/*A* ratio plot for the TRMM Brazil deforestation study site (corresponding with Figures 2h and 3c).

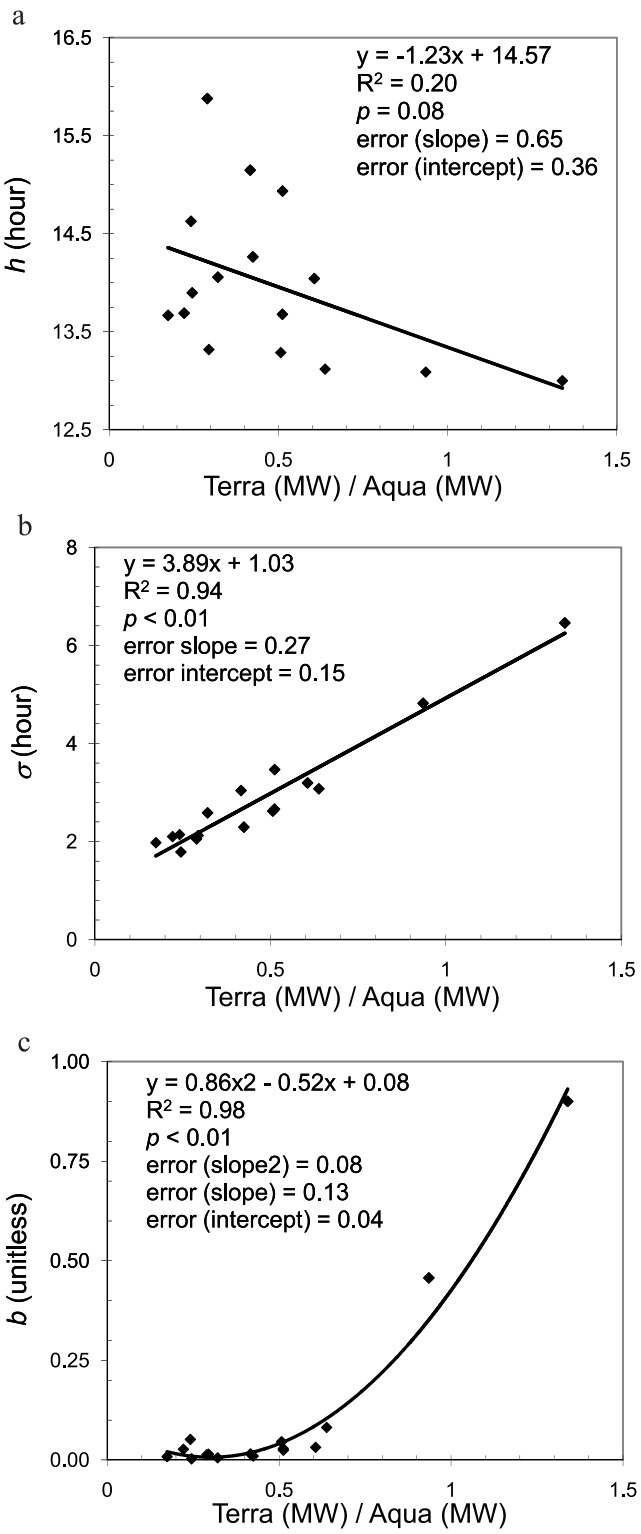

Figure 5. Variation of the peak hour of the diurnal cycle, *h*, as a function of the Terra/Aqua FRP ratio. Note that the relationship is weak ($R^2 = 0.2$) and not significant at $p < 0.05$. Variation of the width of the diurnal cycle, σ, as a function of the Terra/Aqua FRP ratio. The σ value (in hours) corresponds with the width of the curve at half-maximum FRP. Variation of the background level of the diurnal cycle, *b*, as a function of the Terra/Aqua FRP ratio.

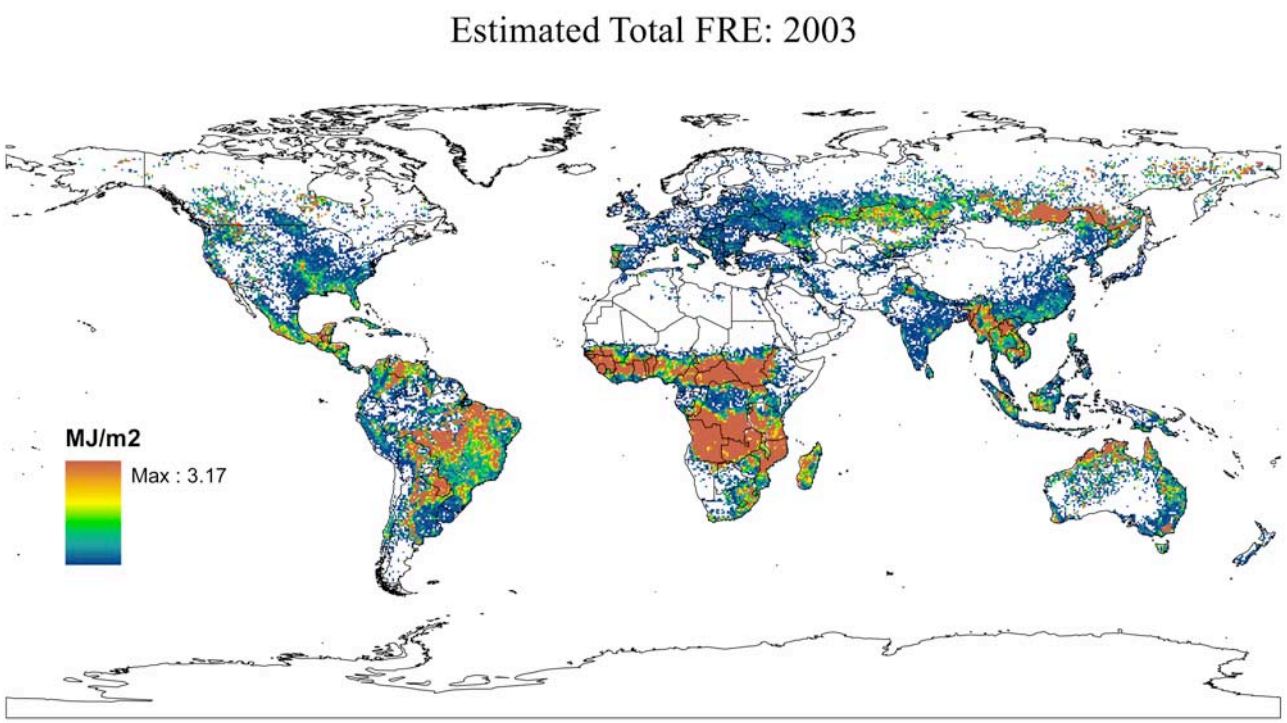

Figure 6. Estimated 2003 FRE (MJ/m^2) from Aqua MODIS. Integrated energy was calculated from FRP (MW) values derived from a Gaussian function using modeled parameters.

enough to encompass temporal variability and offer a statistically robust sample, while being small enough to capture spatial differences (Figures 2a–2h). TRMM VIRS data, provided by *Giglio* [2007], offered additional sites in tropical and subtropical regions, as well as the opportunity to compare diurnal cycles with SEVIRI for overlapping regions in Africa. In addition, we included MODIS daily FRP (MOD14) retrievals from high-latitude boreal sites in Russia and North America (Figures 2b and 2c). These retrievals were included to aid in characterizing the fire cycle beyond the geographic coverage offered by SEVIRI and TRMM (i.e., tropics and subtropics) and therefore provide insight into different fire energy emission cycles. As mentioned previously in section 2.1, MODIS is on polar-orbiting satellites and subsequently provides more frequent retrievals at higher latitudes. Although this bias is accounted for in the gridded CMG product [*Giglio et al.*, 2006], the daily observation bias aids our analysis of the diurnal cycle by providing additional retrievals beyond the nominal overpass times. On average, we found each satellite provided 6 overpasses per day at high latitudes.

[28] FRP observations were binned in hourly increments and normalized by the number of days in the month contributing to a binned hour. Several examples of the diurnal cycle are illustrated in Figure 3.

[29] Using the data described above we found that a modified Gaussian function (equation (5)) provided a simple and accurate representation of the observed diurnal cycle:

$$FRP(t) = FRP_{peak}\left(b + e^{-\frac{(t-h)^2}{2\sigma^2}}\right) \quad (5)$$

Where t is time (hour) for which the discrete FRP is estimated and FRP_{peak} is the peak of the curve. The hour (h) of peak FRP generally occurs in the early afternoon, but this variable has little effect on the final FRE derivation. More importantly is σ, which is the sigma (standard deviation) of the curve and provides details about the duration of fire activity. Equation 5 also includes a background FRP, b, which is a constant independent of time. The dependence of parameters of the diurnal cycle, h, σ, and b, were examined as a function of Terra-to-Aqua FRP (T/A) ratios. The T/A ratio is based on monthly CMG FRP values for 2003–2007 (n = 60) and represents the average ratio between Terra and Aqua FRP retrievals within a given region (Table 1). As stated in section 2.1, the CMG FRP product is the summation of daily MODIS retrievals constituting daytime and nighttime fire detections. Figures 4a–4c show the Terra and Aqua monthly mean FRP plotted for the 60 months of data for several sites.

[30] Our contention is that given the simple Gaussian form adopted for the diurnal cycle, the variation in the T/A ratio can serve as a proxy for the fire energy diurnal cycle. Aqua's afternoon (1330 local time) overpass should correspond (generally) with the hour of peak fire energy. This is a function of local fire weather conditions as humidity decreases and fuels dry with an increase in ambient temperature and preheating by neighboring combusting fuels [*Whelan*, 1995]. Terra's morning overpass will likely correspond with less fire activity as compared with Aqua. We theorize that the ratio between Terra and Aqua FRP should relate to the variables in the Gaussian function, specifically the duration of peak activity (σ parameter) and the constant (background) fire energy (b). In addition, the Gaussian model appears adaptive to local diurnal cycles of fire radiative energy, as illustrated in Figure 3. A large difference between Terra and Aqua (e.g., 0.20 T/A ratio) would indicate a rapid increase in fire radiative energy and shorter

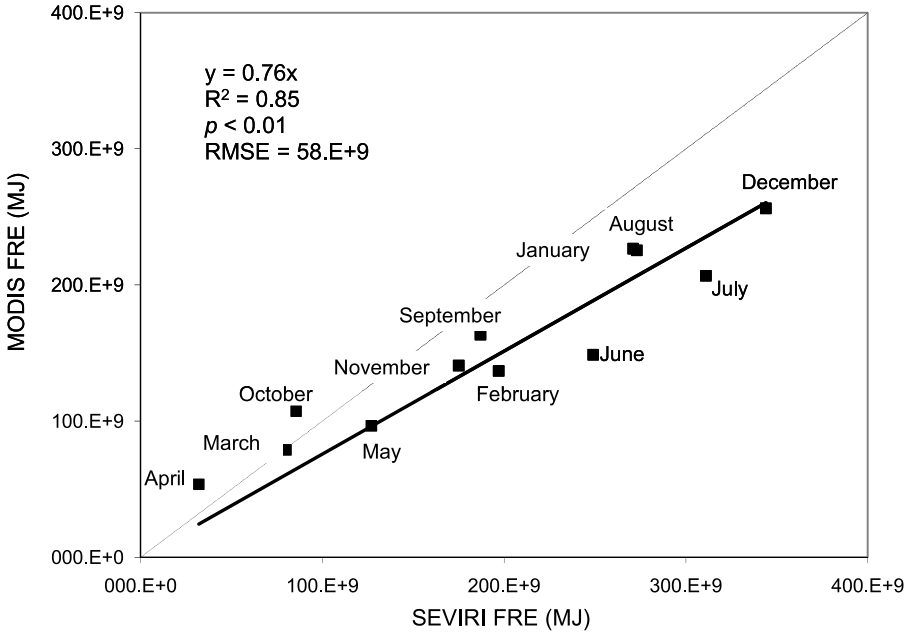

Figure 7. FRE comparison for Africa 2004 between MODIS, estimated using our parameterization method described in this paper, and SEVIRI from the study of *Roberts and Wooster* [2008, personal communication]. The results, both the slope and RMSE, indicate that we underestimate the SEVIRI FRE by roughly 30%. The dashed 1:1 line is shown for reference.

duration of fire activity. Anthropogenic fires such as for pasture maintenance, agricultural clearing, or slash burning, offer a good example as they are typically set during early to mid-day and burn out by evening. A T/A ratio approaching 1.0 would represent a flatter, smoother fire radiative energy cycle where the fire is more active around the clock. Forest fires, particularly fires that are unmanaged, may burn with a relatively (to anthropogenic fires) consistent fire radiative energy throughout the diurnal cycle with a dip in energy in the cooler, often humid, early morning hours [*Whelan,* 1995]. This is evident in the CMG product when the Terra summation of FRP (1030 and 2230) is nearly the same, or even greater, than the Aqua summation (1330 and 0130). Boreal fires, which tend to burn for days to weeks with relatively consistent fire energy emissions, offer a good example of this scenario. In fact, ratios greater than 1.0 are possible, as seen in Figure 4b. In this case, because of changes in local weather conditions fires tend to subside in activity in the early morning hours as would be observed by Aqua at 0130. The result is that the sum of day and night FRP from Terra is greater than the sum of day and night FRP from Aqua.

[31] Figures 5a, 5b, and 5c show, respectively, the variation of the diurnal cycle parameters h, σ and b as a function of the T/A ratio derived from the 2003–2007 period. The σ parameter shows a good correlation with the T/A ratio, highlighting that with low T/A values the width of the curve decreases (i.e., steeper curve), likely associated with rapid burning fire events. On the other hand, as the T/A ratio approaches 1.0 there is a correspondingly wider curve and thus greater σ value. The peak hour (h) of the diurnal cycle is not correlated with the T/A ratio, but values tend to fall around the expected range of early afternoon. A sensitivity test of the h parameter indicated that its influence on calculating FRE was minimal. The background level of the diurnal cycle, b (Figure 5c) shows a small level of constant FRP for most fires sampled over Africa (less than 0.1). However, substantial background is observed over the boreal sites with b nearly 1.0 for T/A ratio. This is indicative of fires that burn more continuously (i.e., day and night).

[32] It should be noted that the diurnal cycle characterization is based on observations made using SEVIRI, TRMM, and two high-latitude regions for MODIS. Application of this process to other regions will include some amount of error and this uncertainty is discussed later in the paper.

3.3. Computation of the FRE From Aqua CMG FRP and T/A Ratio

[33] For a given location, we used the 2003 Aqua FRP from the monthly CMG product described in section 2.1. We chose the CMG because it offers a global-scale data set necessary for comparison with the OCBC inversion product, as well allowing an output product which is appropriate for use with climate models, while retaining temporal and spatial resolution adequate for regional discrimination of fire activity. The Aqua FRP represents the sum of the FRP obtained during the day and night overpasses, therefore we can write the following equation adopted for the fire diurnal cycle described in the previous section:

$$AquaCMGFRP = FRP_{peak}\left[\left(b + e^{-\frac{(13.5-h)^2}{2\sigma^2}}\right) + \left(b + e^{-\frac{(01.5-h)^2}{2\sigma^2}}\right)\right] \quad (6)$$

[34] $AquaCMGFRP$ is the total (mean × cloud-and-overpass–corrected pixel count) FRP value from the CMG product.

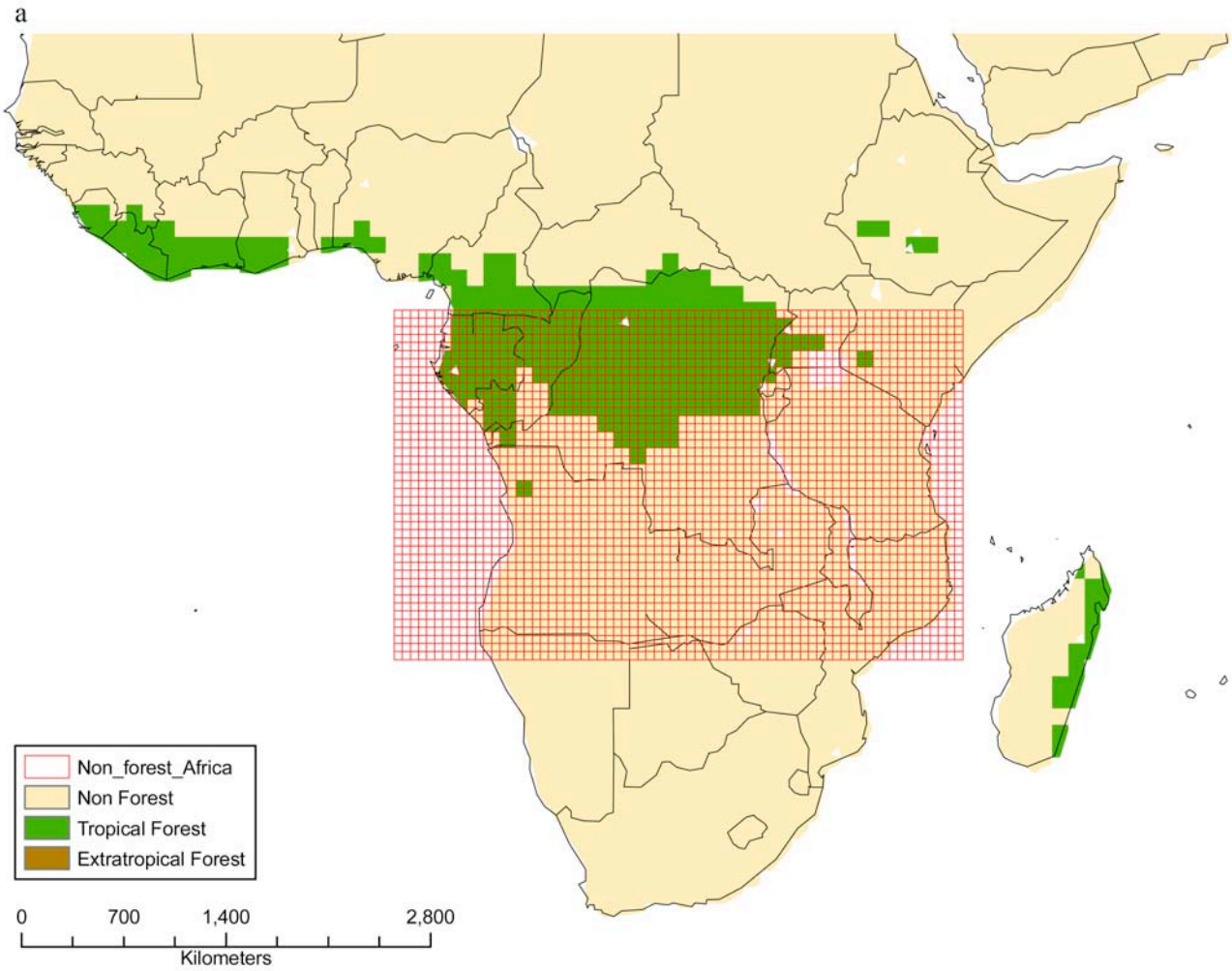

Figure 8. The following figures show the emission coefficient sites used to compare FRE and the inversion-based OCBC emissions to determine an appropriate emission coefficient. Comparisons were performed for 3 different biomes based on the vegetation categorization used by *van der Werf et al.* [2006] and available in the GFEDv2 (see Figure 2). (a) "Non-tropical" site (corresponding with savanna/grassland vegetation), (b and c) tropical forest sites (this is the same as the IGBP's landcover 2), and (d and e) extratropical forest sites.

[35] There are two reasons to justify not setting FRP_{peak} to be equal to the Aqua CMG FRP; (1) as stated, this value is the summation of *both* day and night fire retrievals and cannot be assumed to be just the daytime peak FRP, and (2) although the Aqua afternoon (1330) overpass roughly corresponds with peak fire activity, there is a range of hours over which the true peak may occur (e.g., 1300 to 1800 local hour) as reported by *Giglio* [2007].

[36] We compute FRP_{peak} in two steps (1) Using the T/A ratio we estimate b,h, and σ using the empirical relationship derived in section 3.1 (Figures 5a–5c). (2) We then used the b, h and σ to compute FRP_{peak} using equation (7) (below).

$$FRP_{peak} = \frac{AquaCMGFRP}{\left(b + e^{-\frac{(13.5-h)^2}{2\sigma^2}}\right) + \left(b + e^{-\frac{(01.5-h)^2}{2\sigma^2}}\right)}. \quad (7)$$

[37] The fire radiative energy (FRE) is then computed as:

$$FRE = \int_0^{24} FRP_{peak}\left(b + e^{-\frac{(t-h)^2}{2\sigma^2}}\right) \quad (8)$$

[38] Estimated global annual FRE for 2003 is shown in Figure 6. A comparison of our FRE estimated from Aqua MODIS (650×10^9 MJ) for July, August, September and October 2004 and FRE calculated by *Roberts and Wooster* [2008] from SEVIRI (921×10^9 MJ), for the same period and corresponding area in southern Africa, reveals that our calculation appears consistent. The FRE calculated from SEVIRI by *Roberts and Wooster* [2008] has been divided by 0.55 to account for underestimation of FRP compared with MODIS due to differences in spatial resolution. In addition, FRE from MODIS and SEVIRI has been divided by 0.89 to account for assumed atmospheric transmission

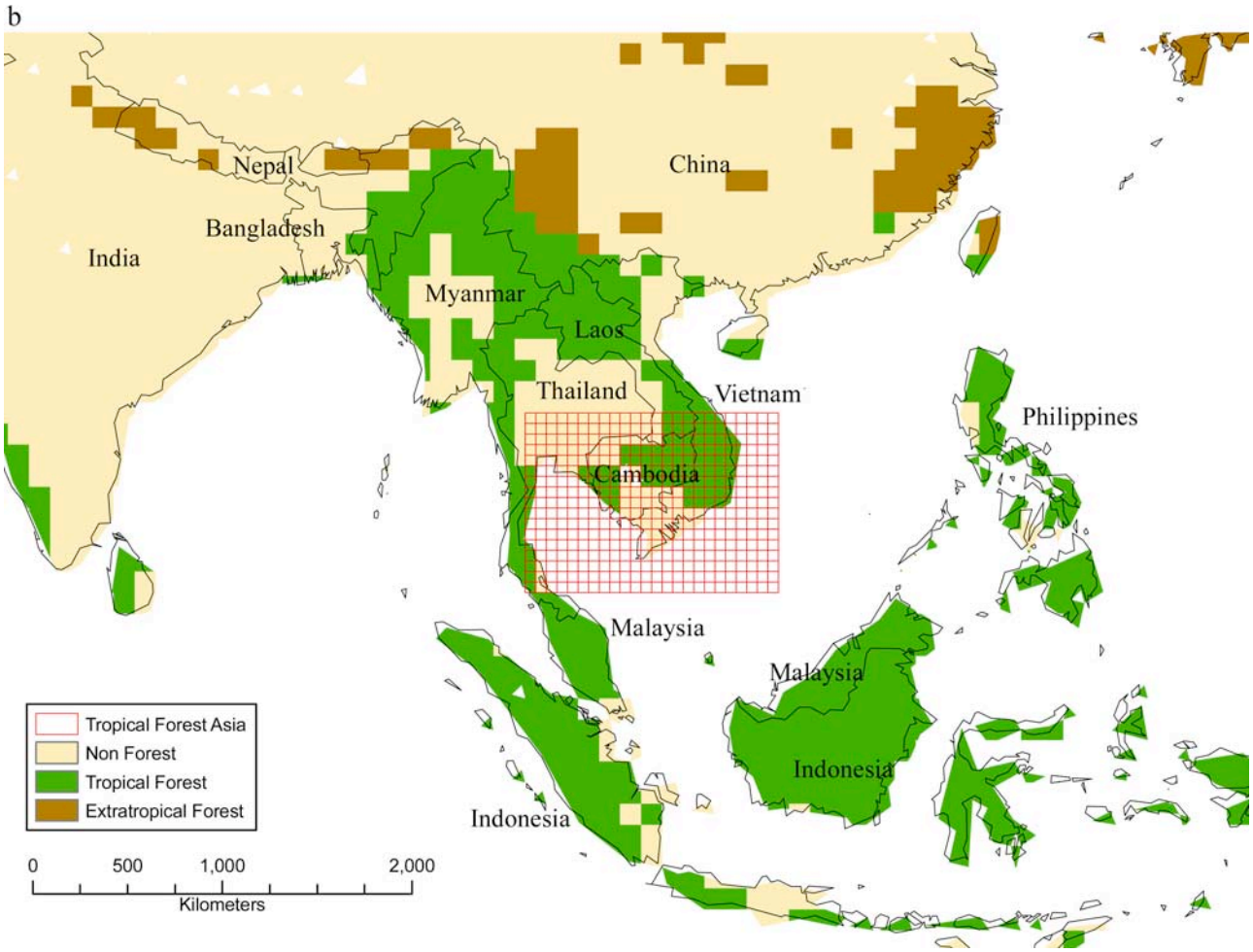

Figure 8. (continued)

perturbation. Using 12 months of FRE estimates from MODIS and SEVIRI, Figure 7 shows that we underestimate the fire radiative energy from MODIS by about 30% compared with SEVIRI. It should be clear that although we use SEVIRI data to develop the temporal trajectory of FRP this does not influence the magnitude of the actual discrete estimates of FRP we make using MODIS.

4. Emission Coefficient

[39] The emission factor is generally defined as the amount of gas or particulate matter emitted (g) per mass of fuel consumed (kg). The factors are typically based on extensive field and laboratory validation and applied across similar biomes [*Andreae and Merlet*, 2001]. Evaluation of uncertainty in emission factors [*Robinson*, 1989] and the wide range of values reported in the literature [*Andreae and Merlet*, 2001; *Chin et al.*, 2002, 2007; *Freeborn et al.*, 2008], suggests emission factors vary naturally by at least 30%.

[40] In their research on rates of energy and aerosols released from fires *Ichoku and Kaufman* [2005] explained that replacing the fuels consumed (M) in equation (1) with FRE necessitates that the emission factor must be based on fire energy. Thus an emission factor for OCBC is expressed using g/MJ instead of g/kg. We refer to this as the *Emission Coefficient* (*EC*) to avoid any confusion with the traditional term.

[41] The FRE (section 3.3) and OCBC emission product (section 2.3) were compared over multiple sites (Figure 8) and constrained by vegetation type (Figure 2), as described by *van der Werf et al.* [2006]. The latter includes three broad categories: savanna/grassland (nonforest), tropical forest, and extratropical forest.

[42] Over southern Africa the area chosen for the analysis contained 95% grassland/savanna fires and 5% tropical forest fires and was used to derive the grassland/savanna emissions coefficient (see Figure 9a) which was estimated to be 2.7 g/MJ with an uncertainty of 0.3 g/MJ. We can convert this emission coefficient to an emission factor using an energy-to-mass conversion factor of 0.41 ± 0.04 kg/MJ which is the average of the 0.368 ± 0.015 kg/MJ and 0.453 ± 0.068 kg/MJ values found in two different studies [*Wooster et al.*, 2005 and *Freeborn et al.*, 2008, respectively]. Dividing the emission coefficient by the energy-to-mass combustion factor yields an emission factor of 6.6 ± 1.0 g/kg for OCBC. This is roughly a factor of two higher than the value suggested by *Andreae and Merlet* [2001] for savanna/grassland (OCBC [TC] 3.7 ± 1.3 g/kg). However, if we convert the emission factors for PM2.5 published by

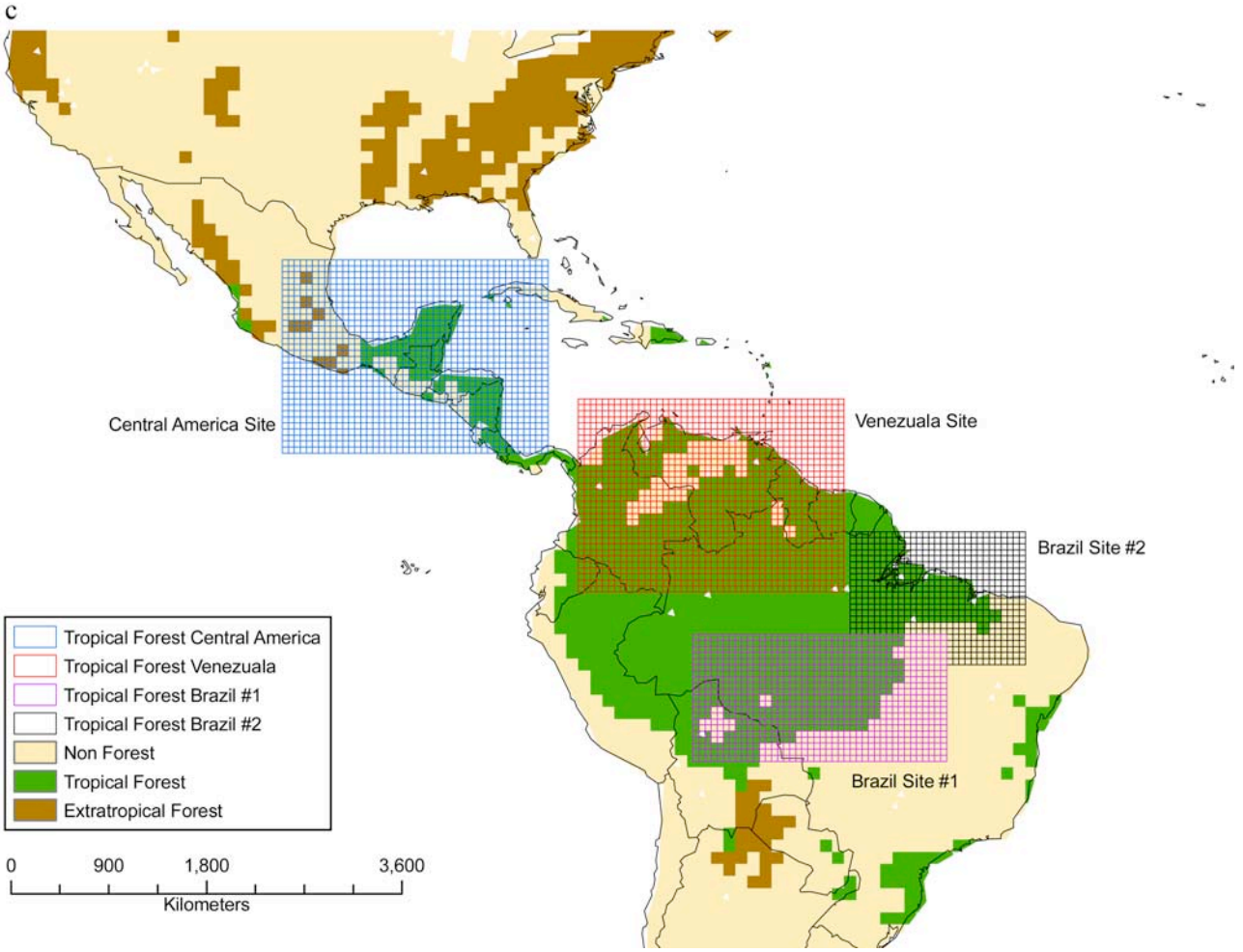

Figure 8. (continued)

Reid et al. [2005] for "Savanna/Grass" and "Woody Savanna and Cerrado" to OCBC using a 0.68 fraction of OCBC in PM2.5 we obtain 4.5 ± 1.0 g/kg and 5.8 ± 1.4 g/kg, respectively, which tends to agree better with our emission factor given the error bars on our estimate.

[43] For tropical and extratropical sites (Figures 8b–8c and 8d–8e, respectively) we applied a correction to reduce the OCBC emission (per cell) to account for the fraction which was emitted from fires occurring in the grassland/savanna biome category. The average grassland/savanna fraction was 30% in tropical forests and 15% in the extratropical forests.

[44] Figure 9b shows the derivation of the tropical forest emission coefficient from 5 sites distributed over Brazil (2), Venezuela (1), Mexico (1), and Southeast Asia (1). Despite regional variability the emission coefficient was estimated to be 8.6 g/MJ with an uncertainty of 0.75 g/MJ. Once converted to an emission factor it equals a value of 21 ± 2.7 g/kg, which is again much larger than the value suggested by *Andreae and Merlet* [2001] (6.6 g/kg), this time by a factor of 3. As a point of comparison, our emission factor estimate is closer to that of *Reid et al.* [2005] (8.3 ± 3 g/kg) and the 11.5 g/kg average tropical forest emission factor recently measured by *Yokelson et al.* [2008]. Once again, this assumes 0.68 fraction of OCBC in PM2.5.

[45] Finally, one site over Southeast Australia and one site in the Lake Baikal region (Russia) were used to derive the OCBC emission coefficient for extratropical forests. Figure 9c shows the relationship between OCBC emissions and FRE over these sites. The coefficient obtained was 14.4 g/MJ with an uncertainty of 0.8 g/MJ. The conversion to an emission factor yields 35.1 ± 3.4 g/kg which is higher by a factor of ∼3–6 than that of *Andreae and Merlet* [2001] (6.1–10.4 g/kg). For the boreal forests *Reid et al.* [2005] suggested an emission factor of 11 ± 3.5 g/kg

[46] Several reasons could explain the discrepancies between the emission factors in the study of *Andreae and Merlet* [2001] and the ones derived in this study: (1) The emission coefficients are based on satellite observations that are not representative of fresh smoke emissions but aged by several hours or days that may have result in significant mass increase of the aerosol through secondary aerosol formation [*Grieshop et al.*, 2008; *Yokelson et al.*, 2008]; (2) the fact that the FRE is systematically underestimated because of cloudiness [*Schroeder et al.*, 2008]; (3) canopy obscuration of fire radiative energy, especially in extratropical understory fires; (4) the limitation of the empirical

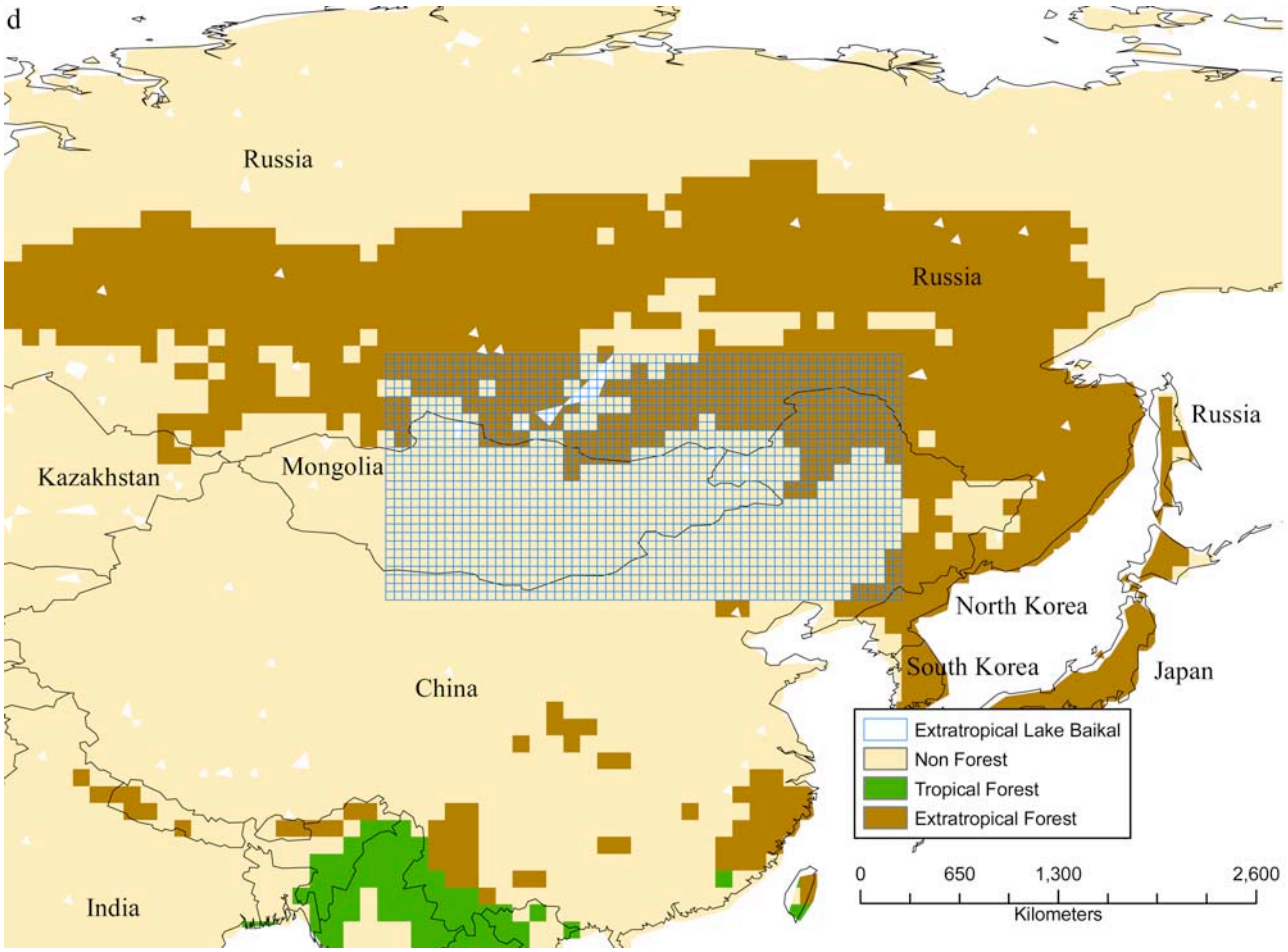

Figure 8. (continued)

formula used to estimate FRE; and (5) the conversion of emission coefficient to emission factor which is at least uncertain by 10% and may vary from biome to biome as the mechanisms regulating the partitioning of the radiative, latent and conductive heat may vary.

5. Error Budget

[47] Several sources of error impact the accuracy of our estimate, especially when it comes to the AOT based OCBC emission product, which is computed indirectly from the MODIS fine mode aerosol optical thickness product. We identified these sources (Table 2) and computed an estimate of the uncertainties for our OCBC emissions estimates, the emissions factors (section 4), and our estimate of the global aerosol burden which is the input for computing the direct radiative forcing.

[48] The first error source is related to the error in the characterization of the fire radiative energy diurnal cycle that impacts the accuracy of the FRE. Comparison of SEVIRI and MODIS, previously shown in section 3.3 and Figure 7, shows a 30% RMSE which can be attributed to errors in the retrievals from both instruments. Therefore the number used in the error budget (a in Table 2) is set to the quadratic average ((30%)/($\sqrt{2}$)), or 21%.

[49] The accuracy of the empirical formula for computing FRP has been evaluated by *Kaufman et al.* [1998] who showed a potential error of 16% using 150 simulated mixed-energy fire pixels. As a corollary, *Wooster et al.* [2003] found theoretical accuracy (RMSD) of 65 $\times$ 10^6 J over a range of 0 to 2000 $\times$ 10^6 J (or 6.5% for the average) using their MIR FRE approach. This accuracy estimate was confirmed by the agreement between the BIRD and MODIS independently derived FRP (15%). This error could actually be larger for certain fires since the lower spatial resolution of MODIS appears to prohibit the less intensely radiating fire pixels from being detected. Thus MODIS underestimates FRE for these fires by up to 46% in comparison to BIRD.

[50] In addition, the MODIS FRP algorithm does not account for water vapor absorption in the 4 μm region of the spectrum, for which the impact is both dependent on the observation angle and the total amount of water vapor, and therefore variable. *Roberts and Wooster* [2008] applied a constant correction factor of 0.89 to the SEVIRI data over southern Africa for an observation angle close to nadir. For MODIS we estimated the error to be 15% based on the fact that the view zenith angle can vary from nadir to 60°.

[51] Cloud obscuration impacts FRP estimates through the fact that fires are not detected (omission error). The 11% estimate of omission errors for MODIS fire detections made by *Schroeder et al.* [2008] over the Amazon region is likely a conservative estimate of the impact given the FRP CMG includes cloud correction [*Giglio*, 2005; *Giglio et al.*, 2006].

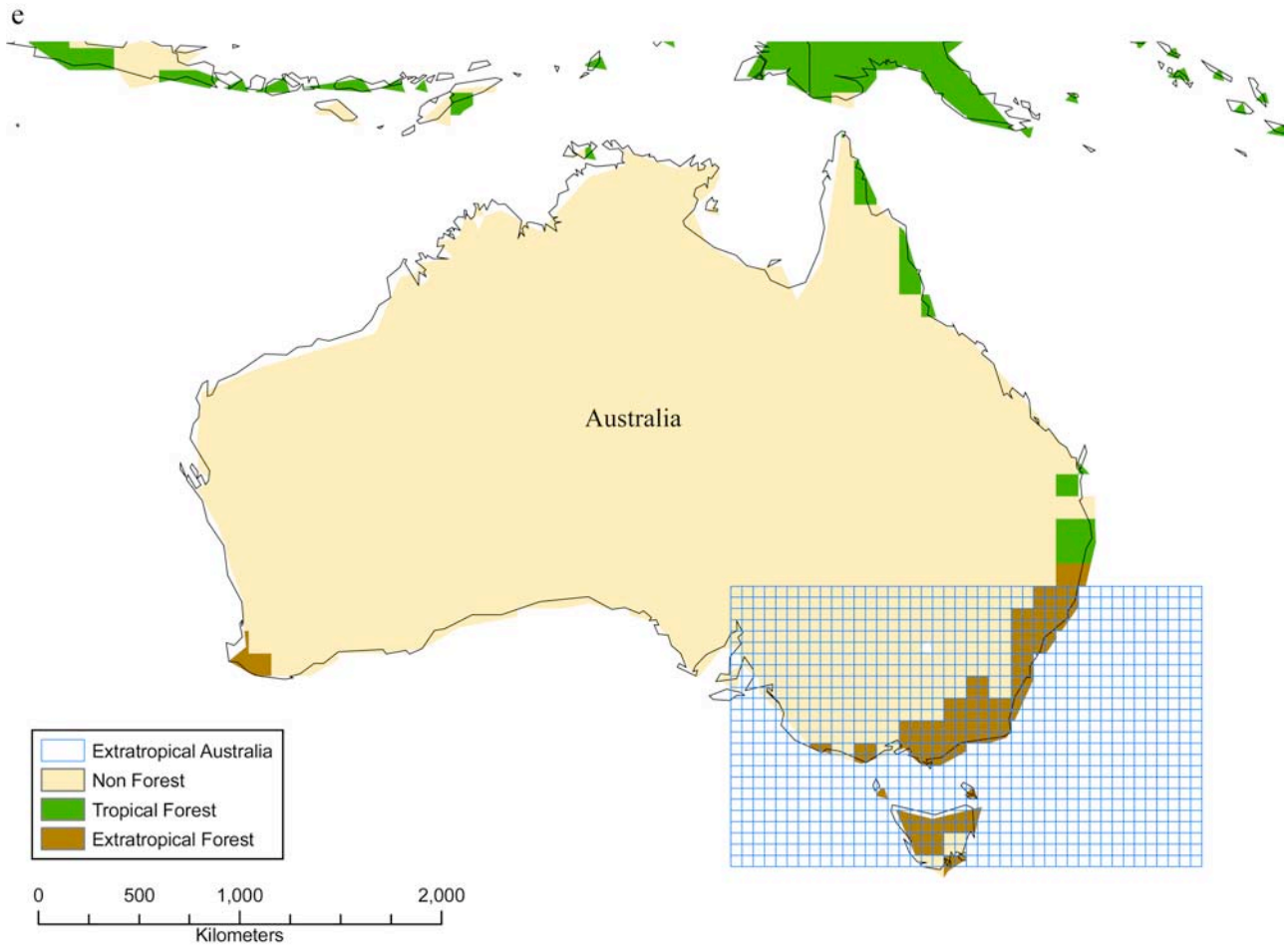

Figure 8. (continued)

Along these same lines, *Hawbaker et al.* [2008] found that MODIS omission rates of small active fires were 73% for Aqua and 66% for Terra. Fires may be missed because of rapid burning, cloud cover, or simply because of spatial scales. However, *Hawbaker et al.* [2008] reiterates the point made by *Kaufman et al.* [1998] that these small fires likely have a small impact in terms of total emissions.

[52] The accuracy of aerosol optical thickness (AOT) measured by MODIS, determined on the basis of comparisons with AERONET Sun photometer measurements, was estimated to be 0.05 + 15% over land and better over ocean [*Levy et al.*, 2007; *Remer et al.*, 2002]. The fine mode AOT accuracy is degraded to 0.05 + 20% (Levy, personal communication 2008). Therefore, assuming a mean AOT of 0.5, we used estimate an error of 30%.

[53] The fine mode AOT was converted to PM2.5 dry mass using a value of 7.6 m^2/g for the mass extinction efficiency (β_e). This value assumes a fixed proportion of carbon in the PM2.5, as well as a particular density and relative humidity [*Chin et al.*, 2002]. Another source of error comes from the conversion of PM2.5 to OCBC using a fraction of 0.68. For example, *Andrea and Merlet* [2001] reported a range of 0.5 to 0.8 OCBC in PM2.5. Given all these factors, we assumed an overall error of 25% on the fine mode AOT to OCBC mass conversion.

[54] Secondary aerosol processes, such as the production of organic aerosol from the photooxidation of volatile organic compounds abundant in biomass burning emissions [*Grieshop et al.*, 2008], are difficult to account for and represents a potentially large error source. We used an error of 25% for that category, recognizing that this error might be larger.

[55] The inversion of the emissions sources is dependent on how well the GOCART model accounts for the different processes. A measure of the accuracy, based on how well the MODIS and GOCART aerosol optical thickness measurements agree, was estimated to be 12% according to *Dubovik et al.* [2008].

[56] We made use of the FRE to combusted biomass conversion in order to convert our emission coefficients to emission factors. The conversion coefficient was originally published by *Wooster et al.* [2005] to be 0.368 g/MJ, but has recently been evaluated to 0.453 g/MJ by *Freeborn et al.* [2008], showing a potential error of 10%.

[57] Using the different error sources in Table 2, we calculated an accuracy of 58% for our estimate of OCBC, with a similar error for the emission factors. Biomass combusted error was much lower (34%), while the error for an estimate of global fine mode AOT using our approach would be 34%. The smaller error in fine mode AOT relative to OCBC is because the conversion to mass [f and g in Table 2] is not necessary, and thus less error is introduced. This is an important point because it is fine mode AOT which is used to calculate the radiative forcing impact from

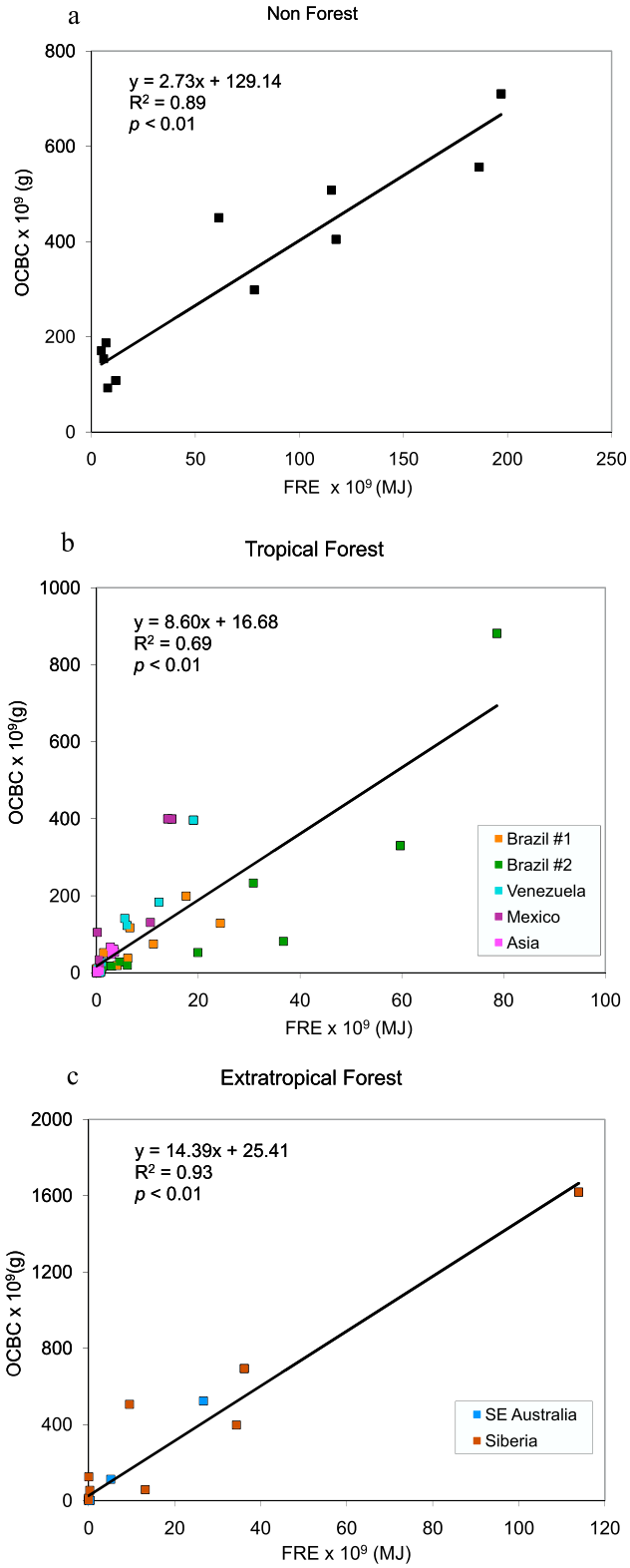

Figure 9. Relationship between monthly estimates of FRE and inversion-based OCBC for savanna/grassland biome (see Figure 8a) from southern Africa. Relationship between monthly estimates of FRE and inversion-based OCBC for the tropical forest biome sites (see Figures 8b and 8c). Relationship between monthly estimates of FRE and inversion-based OCBC for the extratropical forest biome (see Figures 8d and 8e) from Russia and Australia.

biomass burning and thus less uncertainty is associated with the effects of fire on Earth's energy balance.

6. Results and Discussion

[58] Using the monthly FRE product computed in section 3.3 and the emission coefficients computed in section 4 we produced a global OCBC emissions estimate for 2003 from biomass burning (Figure 10). We calculated 18.8 Tg of OCBC emitted from biomass burning globally in 2003. This is lower than, but within the error bars (50%), the 29.6 Tg of OCBC estimated by *Generoso et al.* [2007] for 2003 using a "top down" modeling approach and the 26.1 Tg reported in the Global Fire Emissions Database (GFEDv2, 2005) (GFEDv2 data available at http://ess1.ess.uci.edu/~jranders/data/GFED2/.).

[59] For comparison purposes we adopted the region map (Figure 11) used by *van der Werf et al.* [2006]. Africa (SHAF and NHAF) produced the greatest source of OCBC emissions (4.9 Tg) in 2003 accounting for nearly 26% of the global burden. This is approximately half of what is estimated in the GFEDv2 (9.2 Tg). Annually, Africa usually accounts for 50% of fires detected globally [*Dwyer et al.*, 2000] and roughly half of the vegetation burned [*Bond et al.*, 2004]. However, 2003 was atypical. Fire events in other regions, especially Russian fires [*Kasischke et al.*, 2005], made significant contributions to atmospheric emissions, effectively altering the proportion of emission sources.

[60] Emissions from regions defined as boreal North American (BONA) and boreal Asia (BOAS) contributed the greatest amount of OCBC (28% or 5.3 Tg). Much of this was due to the large-scale fire event near Lake Baikal. Indeed, the Lake Baikal regional fires [40–90°N; 60–180°E] of 2003 were responsible for 4.3 Tg of OCBC. This is close to the GFEDv2 value of 6.1 Tg of OCBC and similar to *Generoso et al.* [2007] estimate of 5.8 Tg for this same region and time frame.

[61] South America (SHSA and NHSA) contributed to roughly 24% of the global burden of OCBC from fires (4.4 Tg this approach compared to 3.63 Tg for the GFEDv2). Of particular interest is the Arc of Deforestation [*Fearnside and Hall-Beyer*, 2007] which was responsible for 2.9 Tg, or 67%, of all emissions from South America and almost 16% of the global source.

[62] Southeast Asia (SEAS) and Australia (AUST) each produced roughly 6.1% and 5% of the global OCBC emission loads (1.15 Tg and 0.9 Tg, respectively for this approach compared to 0.88 Tg and 1.72 Tg for the GFEDv2).

[63] Tables 3a and 3b provide a global comparison of our OCBC estimates with the GFEDv2 for the period 2001–2007. Years 2001 and 2002 were estimated using Terra FRP which had several data gaps due to instrument problems which likely accounts for some of the underestimation in our approach. We also note that the GFEDv2 accounts for soil organic carbon burning which is less likely to be detected by MODIS and therefore not accounted for in our estimate. This may explain the systematic underestimation in our emissions estimate compared to GFEDv2 over Equatorial Asia (EQAS).

[64] For North and South Africa (NHAF and SHAF), our emission estimate and the GFEDv2 showed a very small

Table 2. Error Budget for Components Used in This Research

Error Sources	Error Estimates	Relative Error (%)
(a) FRE from FRP (diurnal cycle)	Figure 7. SEVIRI comparison	21%
(b) FRP empirical formula	*Kaufman et al.* [1998]	16%
(c) Atmospheric effect on FRP	*Roberts and Wooster* [2008]	15%
(d) Cloud correction FRP	*Schroeder et al.* [2008]	11%
(e) Fine mode Aerosol optical depth (at 0.550_{nm})	Levy (personal communication, 2008)	30%
(f) Conversion of fine mode AOT to mass of OCBC	Estimated for range of OCBC mass in PM2.5, relative humidity and ratio of OC/BC	25%
(g) Secondary aerosol processes	*Estimated error allocation might be larger* [*Grieshop et al.*, 2008]	25%
(h) GOCART inversion	*Dubovik et al.* [2008]	12%
(i) Conversion of FRE to biomass combusted	*Wooster et al.* [2005]; *Freeborn et al.* [2008]	10%
Emission estimate	Quadratic sum (a–h)	58%
Emission factors	Quadratic sum (a–i)	59%
Biomass combusted	Quadratic sum (a–d, i)	34%
Fine mode AOT	Quadratic sum (a–e, h)	34%

interannual variation during the 2001–2007 period (coefficient of variation CV between 0.05 and 0.12) however there is about a factor 2 between the two estimates as already noted for 2003. Comparison of biomass burned in Africa between FRE-based estimates, using the methods described in this paper, and the GFEDv2 found a factor of 3 difference in fuel loads [*Ellicott et al.*, 2009] suggesting this as potential source of discrepancy in emission estimates.

[65] Emissions over boreal North American (BONA) and boreal Asia (BOAS) generally agreed between our estimate and the GFEDv2 except for 2002 for BOAS (1.25 Tg and 4.5 Tg, respectively). In addition, the CV observed in the two estimates for BONA and BOAS (between 0.36 and 0.73) was close and reflects the interannual variability within these two regions.

[66] For the rest of the regions, the agreement between the GFEDv2 and our estimate was good for the entire 2001–2007 period; the average was 9.1 Tg for GFEDv2 and 8.1 Tg for our estimate.

[67] A particularly interesting point to be made is that despite our derived emission factors being between a factor 2 and 6 greater than the ones used in the GFEDv2 by *van der Werf et al.* [2006] (which were based on the study by *Andreae and Merlet* [2001]), our annual global emission estimates are between 23% and 44% less than the GFEDv2. A full investigation of this discrepancy is beyond the scope

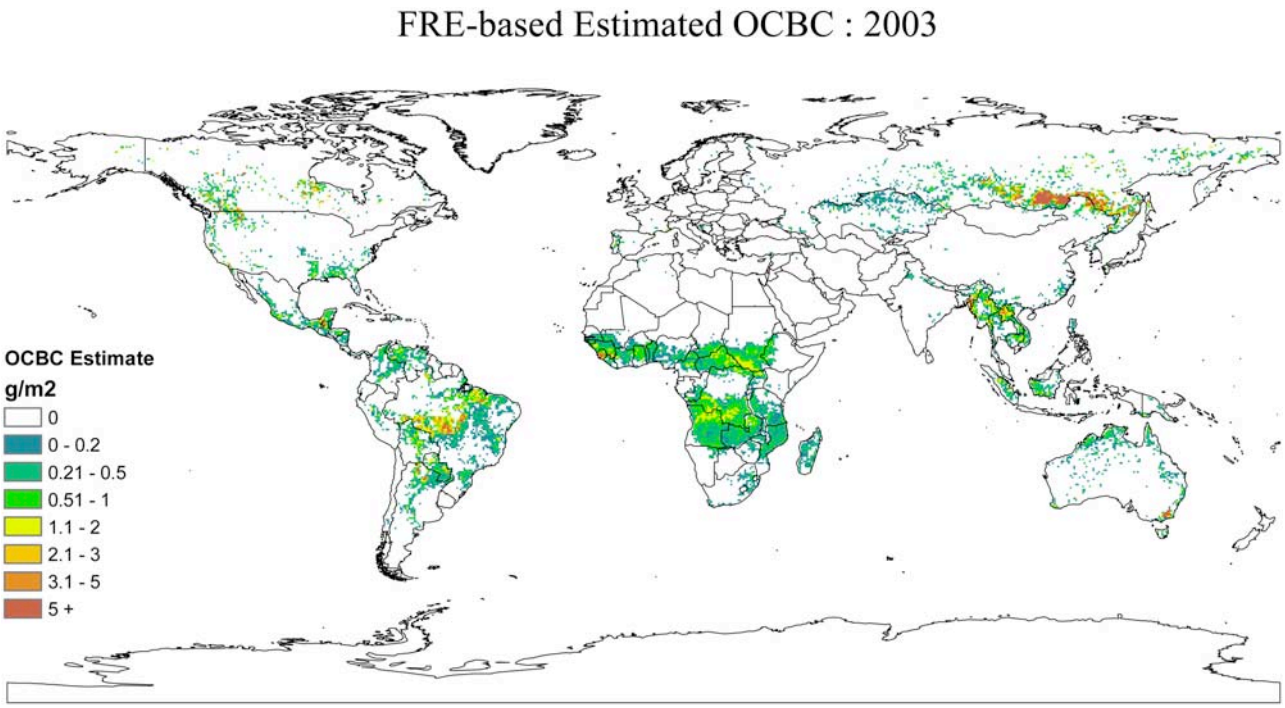

Figure 10. Total OCBC (g/m^2) emissions estimated from biomass burning for 2003. High source regions include eastcentral Brazil, central and southern Africa, Southeast Asia, Central America, and southeast Russia.

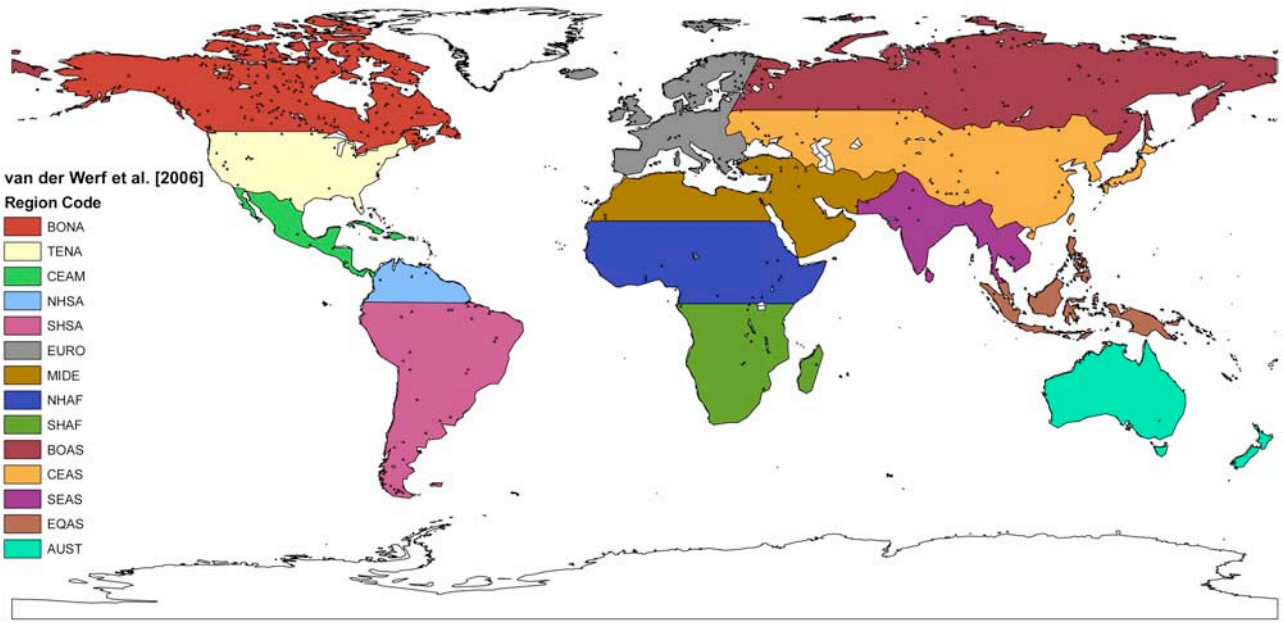

Figure 11. Regions used for comparison of results from this study with the GFEDv2. Regional descriptions are explained in the study by *van der Werf et al.* [2006].

of this paper. While this deviation is still in the uncertainty range derived from our error estimates above, we believe that a more likely explanation is related to uncertainties in the GFEDv2 product, particularly with respect to fuel load assumptions and inaccuracies in the burned area quantification [*Ellicott et al.*, 2009].

7. Conclusions

[68] We have developed an approach to derive FRE from discrete MODIS FRP observations. This method is based on the use of SEVIRI, VIRS, and MODIS data to model the fire diurnal cycle as a modified Gaussian function and relating the parameters of this function to the monthly Terra/Aqua (T/A) ratio of FRP from 16 sites. The T/A ratio were based on the monthly averages of observations within the spatial extent of each site, which varied in size (Table 1). The FRE methodology described in this paper adds value to the limited FRP retrievals made by MODIS and is important to assessing biomass burned and associated emissions. To date, the calculation of FRE from MODIS FRP has not been achieved and therefore this estimate is a first of its kind. Comparison is limited, but initial evaluation against FRE estimated from the geostationary SEVIRI sensor indicates that our approach produces realistic estimates.

[69] From monthly FRE and MODIS AOT based OCBC emission estimates, we derived emission coefficients for three typical biomes: savanna/grassland (2.7 gOCBC/MJ), tropical forest (8.4 gOCBC/MJ) and extratropical forest (14.4 gOCBC/MJ). The coefficient over savanna/grassland tends to agree with previously published values of emission factors, but the values obtained for forest biomes are a factor 4 or 5 higher. Many factors could be responsible for such a discrepancy and deserve further research.

Table 3a. Comparison of Regional (See Figure 11 for Map of Regions) Biomass Burning OCBC Emission Estimates Made in This Research (in Boldface) Versus the GFEDv2 (not in Boldface)[a]

	2001	2002	2003	2004	2005	2006	2007
BONA	**1.00,** 0.19	**0.25,** 0.88	**0.86,** 1.14	**0.86,** 1.32	**0.55,** 0.68	**0.82,** 0.53	**0.60,** 0.41
TENA	**0.69,** 0.34	**0.49,** 0.42	**0.53,** 0.25	**0.34,** 0.25	**0.41,** 0.35	**0.60,** 0.36	**0.92,** 0.60
CEAM	**0.43,** 0.21	**0.37,** 0.33	**0.50,** 0.95	**0.24,** 0.15	**0.55,** 0.40	**0.34,** 0.29	**0.32,** 0.27
NHSA	**0.27,** 0.44	**0.46,** 0.33	**0.47,** 1.08	**0.35,** 0.41	**0.26,** 0.29	**0.26,** 0.28	**0.36,** 0.48
SHSA	**3.48,** 2.74	**2.61,** 3.01	**3.92,** 2.55	**4.78,** 5.29	**4.23,** 5.54	**2.87,** 2.69	**4.21,** 5.85
EURO	**0.04,** 0.41	**0.07,** 0.67	**0.08,** 0.41	**0.05,** 0.48	**0.08,** 0.54	**0.08,** 0.92	**0.08,** 0.48
MIDE	**0.03,** 0.07	**0.03,** 0.08	**0.02,** 0.19	**0.02,** 0.05	**0.02,** 0.06	**0.03,** 0.05	**0.04,** 0.03
NHAF	**2.34,** 6.32	**2.57,** 5.61	**2.41,** 4.63	**2.38,** 4.92	**2.48,** 5.38	**2.19,** 4.53	**2.71,** 5.70
SHAF	**2.32,** 4.79	**2.77,** 4.61	**2.44,** 4.57	**2.48,** 4.55	**2.75,** 4.91	**2.48,** 4.30	**2.49,** 4.35
BOAS	**2.47,** 1.86	**1.25,** 4.50	**4.45,** 6.08	**0.74,** 1.15	**1.26,** 1.17	**1.50,** 2.29	**1.04,** 1.36
CEAS	**0.78,** 0.47	**0.64,** 0.61	**0.68,** 0.39	**0.70,** 0.52	**0.53,** 0.45	**0.61,** 0.53	**0.55,** 0.52
SEAS	**0.76,** 1.89	**0.96,** 0.94	**1.15,** 0.88	**1.52,** 2.05	**1.28,** 1.14	**1.18,** 0.89	**1.53,** 2.91
EQAS	**0.66,** 0.52	**0.25,** 2.76	**0.34,** 1.03	**0.54,** 1.86	**0.46,** 2.82	**0.67,** 4.65	**0.22,** 0.43
AUST	**1.60,** 1.61	**1.94,** 1.37	**0.94,** 1.72	**0.92,** 0.98	**0.45,** 0.53	**1.00,** 1.45	**0.81,** 1.03
Total	**16.87,** 21.86	**14.67,** 26.12	**18.80,** 25.86	**15.91,** 23.98	**15.32,** 24.25	**14.61,** 23.75	**15.89,** 24.41

[a]Values are in Tg OCBC.

Table 3b. Comparison of Regional (See Figure 11 for Map of Regions) Biomass Burning OCBC Emission Estimates Made in This Research (in Boldface) Versus the GFEDv2 (not in Boldface)[a]

	Mean	SD	CV
BONA	**0.71**, 0.74	**0.25**, 0.40	**0.36**, 0.55
TENA	**0.57**, 0.37	**0.19**, 0.12	**0.34**, 0.33
CEAM	**0.39**, 0.37	**0.11**, 0.27	**0.27**, 0.72
NHSA	**0.35**, 0.47	**0.09**, 0.28	**0.27**, 0.59
SHSA	**3.73**, 3.95	**0.78**, 1.52	**0.21**, 0.38
EURO	**0.07**, 0.56	**0.02**, 0.18	**0.24**, 0.33
MIDE	**0.03**, 0.07	**0.01**, 0.05	**0.23**, 0.70
NHAF	**2.44**, 5.30	**0.17**, 0.64	**0.07**, 0.12
SHAF	**2.53**, 4.58	**0.17**, 0.22	**0.07**, 0.05
BOAS	**1.82**, 2.63	**1.28**, 1.92	**0.71**, 0.73
CEAS	**0.64**, 0.50	**0.09**, 0.07	**0.14**, 0.14
SEAS	**1.20**, 1.53	**0.28**, 0.78	**0.24**, 0.51
EQAS	**0.45**, 2.01	**0.19**, 1.52	**0.41**, 0.76
AUST	**1.09**, 1.24	**0.50**, 0.42	**0.46**, 0.34
TOTAL	**16.0**, 24.3	**1.46**, 1.42	**0.09**, 0.06

[a]Values are in Tg OCBC, average, standard deviation, and coefficient of variation over the 2001–2007 period.

[70] The FRE monthly data were then used to estimate OCBC emissions from biomass burning on a global basis. For 2001 to 2007 our annual estimates were close to previously published values, however some regional differences warrant further investigation.

[71] Future work will include refining the FRE and emission coefficient estimates based on the sources of error outlined in the error budget, which indicates an overall uncertainty of ~58%.

References

Andreae, M. O., and P. Merlet (2001), Emission of trace gases and aerosols from biomass burning, *Global Biogeochem. Cycles*, *15*(4), 955–966.

Barrie, L. A., J. Langen, P. Borrell, O. Boucher, J. Burrows, C. Camy-Peyret, J. Fishman, A. Goede, C. Granier, and E. Hilsenrath (2004), The Changing Atmosphere, An Integrated Global Atmospheric Chemistry Observation Theme for the IGOS Partnership (IGACO).

Bond, T. C., D. G. Streets, K. F. Yarber, S. M. Nelson, J. H. Woo, and Z. Klimont (2004), A technology-based global inventory of black and organic carbon emissions from combustion, *J. Geophys. Res.*, *109*, D14203, doi:10.1029/2003JD003697.

Boschetti, L., H. D. Eva, P. A. Brivio, and J. M. Gregoire (2004), Lessons to be learned from the comparison of three satellite-derived biomass burning products, *Geophys. Res. Lett.*, *31*, L21501, doi:10.1029/2004GL021229.

Chin, M., P. Ginoux, S. Kinne, O. Torres, B. N. Holben, B. N. Duncan, R. V. Martin, J. A. Logan, A. Higurashi, and T. Nakajima (2002), Tropospheric aerosol optical thickness from the GOCART Model and comparisons with satellite and Sun photometer measurements, *J. Atmos. Sci.*, *59*(3), 461–483.

Chin, M., T. Diehl, P. Ginoux, and W. Malm (2007), Intercontinental transport of pollution and dust aerosols: Implications for regional air quality, *Atmos. Chem. Phys.*, *7*(21), 5501–5517.

Crutzen, P. J., and M. O. Andreae (1990), Biomass burning in the tropics: Impact on atmospheric chemistry and biogeochemical cycles, *Science*, *250*(4988), 1669–1678.

Dozier, J. (1981), A method for satellite identification of surface temperature fields of subpixel resolution, *Remote Sens. Environ.*, *11*(3), 221–229.

Dubovik, O., T. Lapyonok, Y. J. Kaufman, M. Chin, P. Ginoux, R. A. Kahn, and A. Sinyuk (2008), Retrieving global aerosol sources from satellites using inverse modeling, *Atmos. Chem. Phys.*, *8*(2), 209–250.

Dwyer, E., S. Pinnock, J. M. Gregoire, and J. M. C. Pereira (2000), Global spatial and temporal distribution of vegetation fire as determined from satellite observations, *Int. J. Remote Sens.*, *21*(6–7), 1289–1302.

Ellicott, E., E. Vermote, L. Giglio, and G. Roberts (2009), Estimating biomass consumed from fire using MODIS FRE, *Geophys. Res. Lett.*, *36*, L13401, doi:10.1029/2009GL038581.

Fearnside, P., and M. Hall-Beyer (2007), Deforestation in Amazonia, in *Encyclopedia of Earth*, edited by C. J. Cleveland, Environmental Information Coalition, National Council for Science and the Environment, Washington, D. C., [First published in the Encyclopedia of Earth 15 March 2007; Last revised 30 March 2007; Retrieved 19 January 2009]. (Available at http://www.eoearth.org/article/Deforestation_in_Amazonia)

Freeborn, P. H., M. J. Wooster, W. M. Hao, C. A. Ryan, B. L. Nordgren, S. P. Baker, and C. Ichoku (2008), Relationships between energy release, fuel mass loss, and trace gas and aerosol emissions during laboratory biomass fires, *J. Geophys. Res.*, *113*, D01301, doi:10.1029/2007JD008679.

French, N. H. F., P. Goovaerts, and E. S. Kasischke (2004), Uncertainty in estimating carbon emissions from boreal forest fires, *J. Geophys. Res.*, *109*, D14S08, doi:10.1029/2003JD003635.

García, L., M. J. Lopez, and V. Caselles (1991), Mapping burns and natural reforestation using Thematic Mapper data, *Geocarto Int.*, *1*, 31–37.

Generoso, S., I. Bey, J. L. Attie, and F. M. Breon (2007), A satellite- and model-based assessment of the 2003 Russian fires: Impact on the Arctic region, *J. Geophys. Res.*, *112*, D15302, doi:10.1029/2006JD008344.

Giglio, L. (2005), MODIS Collection 4 Active Fire Product User's Guide: Version 2.2, http://modis-fire.umd.edu/documents/MODIS_Fire_Users_Guide_2.2.pdf, (last accessed 20 September 2008).

Giglio, L. (2007), Characterization of the tropical diurnal fire cycle using VIRS and MODIS observations, *Remote Sens. Environ.*, *108*(4), 407–421.

Giglio, L., I. Csiszar, and C. O. Justice (2006), Global distribution and seasonality of active fires as observed with the Terra and Aqua Moderate Resolution Imaging Spectroradiometer (MODIS) sensors, *J. Geophys. Res.*, *111*, G02016, doi:10.1029/2005JG000142.

Grieshop, A. P., J. M. Logue, N. M. Donahue, and A. L. Robinson (2008), Laboratory investigation of photochemical oxidation of organic aerosol from wood fires. Part 1: Measurement and simulation of organic aerosol evolution, *Atmos. Chem. Phys. Discuss*, *8*, 15,699–15,737.

Hawbaker, T. J., V. C. Radeloff, A. D. Syphard, Z. Zhu, and S. I. Stewart (2008), Detection rates of the MODIS active fire product in the United States, *Remote Sens. Environ.*, *112*(5), doi:10.1016/j.rse.2007.12.008.

Hoelzemann, J. J., M. G. Schultz, G. P. Brasseur, C. Granier, and M. Simon (2004), Global Wildland Fire Emission Model (GWEM): Evaluating the use of global area burnt satellite data, *J. Geophys. Res.*, *109*, D14S04, doi:10.1029/2003JD003666.

Ichoku, C., and Y. J. Kaufman (2005), A method to derive smoke emission rates from MODIS fire radiative energy measurements, *IEEE Trans. Geosci. Remote Sens.*, *43*(11), 2636–2649, doi:10.1109/TGRS.2005.857328.

Innes, J. L. (2000), Biomass burning and climate: An introduction, in *Biomass Burning and Its Inter-Relationships With the Climate System*, edited by J. L. Innes, M. Beniston, and M. Verstraete, pp. 1–13, Kluwer Acad., Netherlands.

IPCC (2007), *Climate Change 2007: The Physical Science Basis. Contribution of Working Group I to the Fourth Assessment Report of the Intergovernmental Panel on Climate Change*, edited by S. Solomon et al., 996 pp., Cambridge Univ. Press, Cambridge, U. K.

Ito, A., and J. E. Penner (2005), Historical emissions of carbonaceous aerosols from biomass and fossil fuel burning for the period 1870–2000, *Global Biogeochem. Cycles*, *19*, GB2028, doi:10.1029/2004GB002374.

Ji, Y. M., and E. Stocker (2002), An overview of the TRMM/TSDIS fire algorithm and product, *Int. J. Remote Sens.*, *23*(16), 3285–3303, doi:10.1080/01431160110070816.

Kasischke, E. S., N. L. Christensen Jr., and B. J. Stocks (1995a), Fire, global warming, and the carbon balance of boreal forests, *Ecol. Appl.*, *5*(2), 437–451.

Kasischke, E. S., N. H. F. French, L. L. Bourgeau-Chavez, and N. L. Christensen (1995b), Estimating release of carbon from 1990 and 1991 forest fires in Alaska, *J. Geophys. Res*, *100*(D2), 2941–2951.

Kasischke, E. S., and J. E. Penner (2004), Improving global estimates of atmospheric emissions from biomass burning, *J. Geophys. Res.*, *109*, D14S01, doi:10.1029/2004JD004972.

Kasischke, E. S., E. J. Hyer, P. C. Novelli, L. P. Bruhwiler, N. H. F. French, A. I. Sukhinin, J. H. Hewson, and B. J. Stocks (2005), Influences of boreal fire emissions on Northern Hemisphere atmospheric carbon and carbon monoxide, *Global Biogeochem. Cycles*, *19*, GB1012, doi:10.1029/2004GB002300.

Kaufman, Y., C. Tucker, and I. Fung (1990), Remote sensing of biomass burning in the tropics, *J. Geophys. Res.*, *95*(D7), 9927–9939.

Kaufman, Y. J., L. Remer, R. Ottmar, D. Ward, R. R. Li, R. Kleidman, R. S. Fraser, L. Flynn, D. McDougal, and G. Shelton (1996), Relationship between remotely sensed fire intensity and rate of emission of smoke: SCAR-C experiment, *Global Biomass*, 685–696.

Kaufman, Y. J., C. O. Justice, L. P. Flynn, J. D. Kendall, E. M. Prins, L. Giglio, D. E. Ward, W. P. Menzel, and A. W. Setzer (1998), Potential global fire monitoring from EOS-MODIS, *J. Geophys. Res.*, *103*(D24), 32,215–32,238.

Korontzi, S., D. P. Roy, C. O. Justice, and D. E. Ward (2004), Modeling and sensitivity analysis of fire emissions in southern Africa during SAFARI 2000, *Remote Sens. Environ.*, *92*(3), 376–396.

Levy, R. C., L. A. Remer, S. Mattoo, E. F. Vermote, and Y. J. Kaufman (2007), Second-generation operational algorithm: Retrieval of aerosol properties over land from inversion of Moderate Resolution Imaging Spectroradiometer spectral reflectance, *J. Geophys. Res.*, *112*, D13211, doi:10.1029/2006JD007811.

Reid, J. S., T. F. Eck, S. A. Christopher, R. Koppmann, O. Dubovik, D. P. Eleuterio, B. N. Holben, E. A. Reid, and J. Zhang (2005), A review of biomass burning emissions. Part III: Intensive optical properties of biomass burning particles, *Atmos. Chem. Phys.*, *5*, 827–849.

Remer, L. A., et al. (2002), Validation of MODIS aerosol retrieval over ocean, *Geophys. Res. Lett.*, *29*(12), 8008, doi:10.1029/2001GL013204.

Roberts, G., M. J. Wooster, G. L. W. Perry, N. Drake, L. M. Rebelo, and F. Dipotso (2005), Retrieval of biomass combustion rates and totals from fire radiative power observations: Application to southern Africa using geostationary SEVIRI imagery, *J. Geophys. Res.*, *110*, D21111, doi:10.1029/2005JD006018.

Roberts, G. J., and M. J. Wooster (2008), Fire detection and fire characterization over Africa using Meteosat SEVIRI, *IEEE Trans. Geosci. Remote Sens.*, *46*(4), 1200–1218, doi:10.1109/TGRS.2008.915751.

Robinson, J. M. (1989), On uncertainty in the computation of global emissions from biomass burning, *Clim. Change*, *14*(3), 243–261.

Robinson, J. M. (1991), Fire from space: Global fire evaluation using infrared remote sensing, *Int. J. Remote Sens.*, *12*(1), 3–24.

Roy, D. P., Y. Jin, P. E. Lewis, and C. O. Justice (2005), Prototyping a global algorithm for systematic fire-affected area mapping using MODIS time series data, *Remote Sens. Environ.*, *97*(2), 137–162.

Schroeder, W., I. Csiszar, and J. Morisette (2008), Quantifying the impact of cloud obscuration on remote sensing of active fires in the Brazilian Amazon, *Remote Sens. Environ.*, *112*(2), 456–470, doi:10.1016/j.rse.2007.05.004.

Schultz, M. G., A. Heil, J. J. Hoelzemann, A. Spessa, K. Thonicke, J. G. Goldammer, A. C. Held, J. M. C. Pereira, and M. van het Bolscher (2008), Global wildland fire emissions from 1960 to 2000, *Global Biogeochem. Cycles*, *22*, GB2002, doi:10.1029/2007GB003031.

Soja, A. J., W. R. Cofer, H. H. Shugart, A. I. Sukhinin, P. W. Stackhouse, D. J. McRae, and S. G. Conard (2004), Estimating fire emissions and disparities in boreal Siberia (1998–2002), *J. Geophys. Res.*, *109*, D14S06, doi:10.1029/2004JD004570.

van der Werf, G. R., J. T. Randerson, L. Giglio, G. J. Collatz, P. S. Kasibhatla, and A. F. Arellano (2006), Interannual variability in global biomass burning emissions from 1997 to 2004, *Atmos. Chem. Phys.*, *6*, 3423–3441.

van der Werf, G. R., J. T. Randerson, G. J. Collatz, and L. Giglio (2003), Carbon emissions from fires in tropical and subtropical ecosystems, *Global Change Biol.*, *9*(4), 547–562.

Whelan, R. J. (1995), *The Ecology of Fire*, Cambridge Univ. Press, New York.

Wooster, M. J. (2002), Small-scale experimental testing of fire radiative energy for quantifying mass combusted in natural vegetation fires, *Geophys. Res. Lett.*, *29*(21), 2027, doi:10.1029/2002GL015487.

Wooster, M. J., B. Zhukov, and D. Oertel (2003), Fire radiative energy for quantitative study of biomass burning: Derivation from the BIRD experimental satellite and comparison to MODIS fire products, *Remote Sens. Environ.*, *86*(1), 83–107.

Wooster, M. J., G. Roberts, G. L. W. Perry, and Y. J. Kaufman (2005), Retrieval of biomass combustion rates and totals from fire radiative power observations: FRP derivation and calibration relationships between biomass consumption and fire radiative energy release, *J. Geophys. Res.*, *110*, D24311, doi:10.1029/2005JD006318.

Yokelson, R. J., T. J. Christian, T. G. Karl, and A. Guenther (2008), The tropical forest and fire emissions experiment: Laboratory fire measurements and synthesis of campaign data, *Atmos. Chem. Phys.*, *8*(13), 3509–3527.

M. Chin, Laboratory for Atmospheres, NASA Goddard Space Flight Center, NASA Code 613.3, Greenbelt, MD 20771, USA.

O. Dubovik, Laboratory of Atmospheric Optics, University of Sciences and Technologies of Lille 1, F-59655 Villeneuve d'Ascq CEDEX, Lille, France.

E. Ellicott and E. Vermote, Department of Geography, University of Maryland, 4321 Hartwick Road, Suite 209, College Park, MD 20740, USA. (eric@ltdri.org)

L. Giglio, Science Systems and Applications, Inc., 10210 Greenbelt Road, Suite 600, Lanham, MD 20706, USA.

T. Lapyonok, Planetary Geodynamics Laboratory, NASA Goddard Space Flight Center, Code 698, Greenbelt, MD 20771, USA.

G. J. Roberts, Department of Geography, Kings College of London, Strand, WC2R 2LS London, UK.